International Journal of Plasticity 107 (2018) 100–121

Contents lists available at ScienceDirect

International Journal of Plasticity

journal homepage: www.elsevier.com/locate/ijplas

A thermodynamically-based viscoelastic-viscoplastic model for the high temperature cyclic behaviour of 9–12% Cr steels

A. Benaarbia*, J.P. Rouse, W. Sun

Department of Mechanical, Materials and Manufacturing Engineering, University of Nottingham, Nottingham, Nottinghamshire NG7 2RD, UK

ARTICLE INFO

Keywords:
Cyclic viscoplasticity
Fatigue-relaxation
High-temperature steels
Thermodynamics of irreversible processes

ABSTRACT

Improving the understanding of the long term rate dependent behaviour of materials is of critical importance in many engineering applications. Without this understanding, it is potentially difficult to ensure safe and effective plant operation while simultaneously satisfying requirements for sustainability and responsible resource management. In the present work, a thermodynamically-based constitutive model is proposed to capture the rate sensitivity, the stress relaxation and the accelerated cyclic softening observed during cyclic deformation of a P91 steel at an elevated temperature ($600°C$). The model is developed within the framework of Thermodynamics of Irreversible Processes and Generalized Standard Materials formalism, thereby offering a thermodynamically grounded coupling of both viscoelasticity (semi-recoverable strain accumulation at vastly different time scales) and viscoplasticity (irreversible strain observed above the stress threshold). The later part combines a hyperbolic sine-power flow rule with non-linear isothermal cyclic evolution of isotropic and kinematic hardening. The applicability of the model to various mechanical loadings (e.g., cyclic tensile-compression tests, fatigue-relaxation tests, anhysteretic tests) is validated by designing a heuristic optimisation program based on a nonlinear least-squares function coupled with the Levenberg-Marquardt algorithm. The optimisation procedure is informed (through the estimation of initial material parameter estimates and objective function evaluation) by anhysteretic type experiential data only (wherein long term load hold periods are introduced at various points in the waveform). Rate dependency is determined and validated by considering experimental waveforms with different loading (strain) rates ($0.1\%.s^{-1}$, $0.01\%.s^{-1}$ and $0.001\%.s^{-1}$) and ranges (0.25%, 0.4% and 0.5%) to highlight most of the deformation mechanisms involved during the fatigue and relaxation processes. By comparing predicted and experimentally observed material responses, it is demonstrated in the present work that the viscoelastic-viscoplastic strain decomposition has the ability to capture the accelerated cyclic softening and the uncoupled stress relaxation behaviour (below and above yielding) for a P91 steel at elevated temperatures.

1. Introduction

Some conventional (sub-critical) power plant components (such as headers and main steam lines) are exposed to elevated temperatures approaching $600°C$. In addition to this, thick walled components may undergo severe temperature variations (during high frequency start up and shut down cycles, “two-shifting”), thereby inducing various damage mechanisms due to thermo-mechanical fatigue, fatigue-relaxation and fatigue-creep solicitations (see. Pineau and Antolovitch (2015)). An improved

* Corresponding author.
E-mail address: adil.benaarbia1@nottingham.ac.uk (A. Benaarbia).

https://doi.org/10.1016/j.ijplas.2018.03.015
Received 16 November 2017; Received in revised form 29 March 2018; Accepted 30 March 2018
Available online 06 April 2018

Nomenclature

Ψ	Thermodynamic potential
Φ^*	Dual dissipation potential
$\underline{\underline{\varepsilon}}$	Total strain tensor
$\underline{\underline{\varepsilon}}_e$	Elastic strain tensor
$\underline{\underline{\varepsilon}}_{vj}$	Viscoelastic strain tensors, with $j = 1,2,3$
$\underline{\underline{\varepsilon}}_{vp}$	Viscoplastic strain tensor
$\underline{\underline{\chi}}_{vj}$	Conjugate variable of $\underline{\underline{\varepsilon}}_{vj}$
$\underline{\underline{\chi}}_{vp}$	Conjugate variable of $\underline{\underline{\varepsilon}}_{vp}$
$\mathbb{C}_e$	Fourth order isotropic elastic tensor
$\mathbb{C}_{vj}$	Fourth order Kelvin-Voigt elastic tensors, with $j = 1,2,3$
$\mathbb{D}_{vj}$	Fourth order isotropic viscous tensors, with $j = 1,2,3$
λ	Viscoplastic multiplier
$\underline{\underline{\alpha}}_i$	Internal variable for kinematic hardening
$\underline{\underline{X}}_i$	Backstress tensor for kinematic hardening
c_i, γ_i	Kinematic hardening constants, with $i = 1,2$
$\underline{\underline{\mathbb{N}}}_{vp}$	Viscoplastic flow direction
K_{vp}	Viscoplastic resistance
m_{vp}	Viscoplastic hardening exponent
f	Yield function
r	Internal variable for isotropic hardening
R	Drag stress for isotropic hardening
Q_1, Q_2, b	Isotropic hardening constants

understanding of such deformation mechanisms and their synergy is therefore indispensable for the design of high-temperature components in power plants if their integrity is to be guaranteed and if optimum plant operation decisions are to be made.

High-Cr steels, including ASME Grade P91 and Grade P92, have long been used as base materials for many high temperature components in sub-critical and supercritical power plants (see. Viswanathan et al. (2005)). These materials are characterized by their high creep strength and enhanced properties of weldability, hardenability, and corrosion resistance (e.g. Swindeman et al. (2004), Chen et al. (2011)). As such, these materials are a popular choice for replacement steam pipe sections and header components in many existing power plants (see Farragher et al. (2013), Li et al. (2016b)). In many countries electricity networks are becoming increasingly de-carbonised, meaning that baseline generation load is provided by renewable sources and traditional thermal power plants (for example, coal and gas) are being called upon to account for the shortfall between supply and demand. In such cases the generation strategies of thermal power plants must be flexible; operators must have the capability to begin generating at full or partial load in a short period of time. These operating requirements necessitate that pipework and header components will operate at both elevated temperatures and under complex cyclic excitations. The loading-unloading waveforms can include long dwell periods (ranging from the order of a few hours to several weeks), thereby causing significant stress relaxation in the component (in addition to elastic/plastic effects). Much of the published literature has focused on the application of elastic viscoplastic type material models (see Barrett et al. (2013), Rouse et al. (2013), Kyaw et al. (2016), etc.), however viscoelastic formulations must be developed if the stress relaxation behaviour is to be properly quantified. The interaction of these different mechanisms (i.e. viscoelastic and viscoplastic) makes the modelling of the mechanical behaviour and the prediction of lifetime of the base materials more complex.

For components subjected to fatigue-creep (and/or relaxation) deformations at high temperatures, the interaction of both processes induces a reduction in the lifetime which remains to be evaluated for small deformations and long dwell periods. Numerous experimental studies have been conducted to understand the combined effects of fatigue including longer and shorter dwell periods (e.g., Kyaw et al. (2016), Xu et al. (2017), Shankar et al. (2017), etc.). The strong interaction between time-dependent (creep viscosity) and time-independent deformation (fatigue plasticity) mechanisms makes the behaviour of 9–12% steels more complex. A significant number of experimental fatigue-relaxation (or fatigue-creep) results are available for P91/P92 steels at elevated temperatures (e.g., Fournier et al. (2008a, b), Cui et al. (2013), Saad et al. (2013), etc.). It should be noted that the loading dwell periods experienced in a component are often relatively long in duration and it is commonly impractical to implement a direct equivalent in the laboratory. The fatigue-relaxation tests presented herein are carried out under dwell periods of the order of 2.5 h. Although these dwell periods remain below those encountered during realistic operational services (there is a need to orientate the study towards a physical modelling that allows the exploration of long dwell periods) they have been determined to be sufficient to illustrate the effects of combined viscoelastic and viscoplastic phenomenon.

The modelling of fatigue-relaxation (and/or fatigue-creep) behaviour of 9–12% Cr steels is still an open topic (e.g., Fournier et al. (2011), Wang et al. (2015), Zhang and Aktaa (2016), Zhang and Xuan (2017), etc.). The modelling process is complicated due to the encountered phenomena (existence of viscoelasticity, viscoplasticity, primary hardening, secondary hardening, etc.), their origin and interactions (mechanical or thermal nature) as well as the type of loading excitation (with or without mean stresses, varied amplitudes, random loadings, uniaxial and/or multiaxial loadings, etc.). However, such modelling holds the key for using these high-Cr steels in structural power plant applications in more intelligent ways. Note that the constitutive modelling framework which deals with creep and cyclic loading conditions of power plant materials has had relatively little attention. The commonly used model is the unified viscoplasticity model initially developed by Chaboche and Rousselier (Chaboche and Rousselier (1983)). This viscoplastic model includes the pioneering works of Prager (1949) and Armstrong and Frederick (1966), and has been used and improved by many researchers in literature (e.g. Chaboche (1989), Ohno and Wang (1993), Yaguchi et al. (2002), Kang et al. (2003), Chen and Jiao (2004), Abdel-Karim (2009), Zhu et al. (2017), etc.). The modelling of plasticity and creep can be split into two broad groups, unified and non-unified theories (e.g. Chaboche and Rousselier (1983), Contesti and Cailletaud (1987), etc.). In unified constitutive models, creep (viscous) and plastic strains are represented by a single inelastic measure and considered to be rate-dependent (e.g. Chaboche (2008), Barrett et al. (2013), Wang et al. (2014), Ahmed et al. (2016), Zhang and Xuan (2017), etc.). Conversely, the non-unified models consider creep strain to be rate-dependent but plastic strain (on the other hand) to be rate-independent; creep and plastic strain are therefore considered to be two separate measures (e.g. Cailletaud and Sai (1995), Velay et al. (2006)). Non-unified models have been found to provide reasonable simulations for the time-dependent ratcheting behaviour for 304 stainless steel

materials when creep is a dominant factor in deformation (see. Kang and Kan (2007)). Such a condition is met when the material is subjected to high temperatures, however deficiencies in predictive capability have been identified for alternative ratcheting loading cases (for example, at room temperature). They are also difficult to implement into finite element code due to the different flow rules involved. Although many constitutive models do exist to represent the behaviour of power plant materials, most of them are elastic-viscoplastic. The prediction of P91 behaviour must couple viscoelasticity and viscoplasticity however as stresses can be shown to relax below the instantaneous "yield" value. This can be checked by uniaxial monotonic tension tests followed by an unloading to zero stress. When such a specimen is kept at zero stress only a part of the total strain can be recovered (regardless of hold time), therefore suggesting that a coupled viscoelastic-viscoplastic model is required.

The development of thermodynamically admissible constitutive models has received great attention in the literature in the past decades. Quite often, continuum mechanics concepts are associated with the thermodynamics of irreversible processes (TIP) in order to define the behavioural constitutive equations. Numerous studies have been devoted to development of thermodynamically-based models for investigating non-linear viscoelastic, viscoplastic and damage behaviour of several materials, especially polymers and metals (e.g., Lemaitre (1985), Chaboche (1997), Voyiadjis and Dorgan (2007), Haddag et al. (2009), Darabi et al. (2011), Al-Rub and Darabi (2012), Yu et al. (2016, 2017), Gudimetla and Doghri (2017), etc). Although the literature in developing thermodynamically-based models is rich and mature, few attempts are available when coupling thermodynamics to the generalized standard materials (GSM) formalism (e.g., Halphen and Nguyen (1975), Ranc and Chrysochoos (2013), Launay et al. (2011), Chatzigeorgiou et al. (2016), etc.). This formalism (widely used elsewhere in the literature) insists on the application of the Clausius-Duhem inequality, such that the constitutive equations can be derived from a free energy potential (state equations) and a dissipation potential (evolution equations). This formalism was first introduced by Nguyen (1973) in 1973 is the basis for the model presented hereafter.

In this paper, a viscoelastic-viscoplastic constitutive model for P91 steel is proposed under isothermal conditions. The model is mainly developed for studying the fatigue-relaxation behaviour at different strain rates/amplitudes and stress relaxation periods. Constitutive equations based on TIP coupled with GSM are derived. The model combines a hyperbolic sine-power flow rule (in the viscoplastic contribution) with non-linear isothermal cyclic evolution of isotropic and kinematic hardening to highlight the irreversible strain evolution for loads above the stress threshold. A significant amount of attention is also given to capture the semi-recoverable viscoelastic effects occurring at different time scales (i.e., short, medium and long-term). Readers are encouraged to note the use of the term semi-recoverable, in relation to viscoelastic deformation. This is done for several reasons and warrants some explanation. Physically, it is of course true that all deformation entails a degree of irreversibility and is therefore not totally "recoverable". In the context of viscoelasticity, deformation is here said to be semi-recoverable in order to refer these effects (viscoelastic strain may be thought of as creep strain experienced by specimens in standard constant low load/stress creep tests, suggesting that it relates to some level of permanent alteration to a material's microstructure) while highlighting that (in the modelling context) total recovery is only possible over very long time periods.

To fulfil the primary objective of the present survey, a brief description of experimental tools and methods used for conducting experiments is first presented. Initial experimental observations are exposed followed by a mechanical analysis of cyclic behaviour to highlight the different physical features exhibited during the deformation process of investigated materials. The theoretical formulation of the constitutive isothermal viscoelastic-viscoplastic model is then presented based on TIP and GSM formalisms. The state and evolution laws are derived from the partial derivatives of thermodynamic and dissipation potentials. An uniaxial validation of the constitutive model is thus presented, with validation based on a heuristic optimisation program combining a nonlinear least-squares function and Levenberg-Marquardt algorithm. It is shown that this program is simple and straightforward and yields unique values for the model material parameters. The last part describes and discusses the results obtained from the uniaxial validation. Several conclusions, drawn from the findings, are finally put forward, along with some proposals regarding future investigations and improvements of the proposed model.

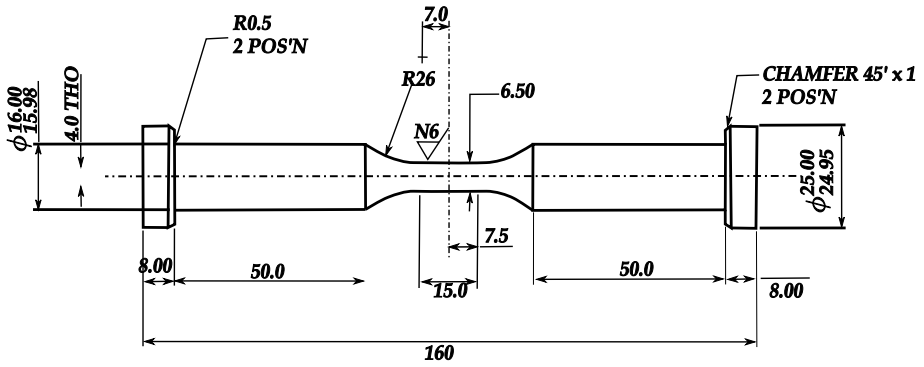

Fig. 1. Geometry of the samples used for experiments (all dimensions in mm).

2. Initial experimental observations and mechanical analysis

2.1. Experimental procedure

All experimental data presented in the current work were gathered for isothermal ($600°C$) conditions using an Instron 8862 test rig fitted with a radio frequency (RF) induction heating system. Solid $6.5mm$ gauge section diameter "button end" specimens were used in all cyclic testing (see Fig. 1), wherein load profiles were specified on a strain basis (strain was monitored during testing with a spring loaded extensometer). In all cases temperature was controlled using type k thermocouples, with axial temperature variations over the sample gauge section verified to be less than $\pm\ 10\ ^oC$ (thereby in compliance with BS ISO 12111-2011; note that the true axial temperature variations observed during testing were less than $\pm\ 1\ °C$). Thermocouples were spot welded to the shoulder of the gauge section for all tests in order to negate concerns over the effects of thermocouple welds on the long term behaviour of a specimen (for example, premature crack imitation at weld locations). Shoulder temperatures are typically cooler than those in the gauge section, therefore a scaling factor was defined in order to correct these measurements to a gauge section equivalent. Calibration samples (i.e. samples with a series of equally spaced thermocouples over the gauge section) were used to *i)*. determine these scaling factors, *ii)*. verify that scaling factors were stable for the duration of a proposed test, and *iii)*. aid in the design of the induction coil (particularly with reference to the temperature uniformity conditions outlined in BS ISO 12111-2011). Load and temperature control was achieved using Instron's MAX software.

Experimental results used in the present work utilise several cyclic loading waveforms in order to investigate and verify various deformation mechanisms that are observed in P91 steel. Standard waveforms have been applied and, for clarity, a brief discussion of these is now presented. The majority of model development is achieved using so called semi-anhysteretic loading waveforms, wherein $2.5hr$ hold periods were applied during the tensile loading region at strain levels equalling 0.1%, 0.2%, 0.3%, 0.4%, and 0.5% (a schematic representation of this can be seen in Fig. 2). Hold period durations were defined such that both short term and long term viscoplastic material behaviours could be determined (i.e. stresses relaxed below the expected yield surface into conditions). Semi-anhysteretic tests used in the present work are fully reversed (i.e. $R = -1$), with strain limits set to $\pm$ 0.5%. Waveforms are described as semi-anhysteretic here as strain hold periods are included only in certain regions of the tensile loading branch (typically anhysteretic waveforms would incorporate compressive hold periods as well). In the interest of space however, semi-anhysteretic waveforms will be refereed to hereafter simply as anhysteretic waveforms. Strain rates were constant for a given anhysteretic waveform and values of $0.1\%.\ s^{-1}$, $0.01\%.\ s^{-1}$, and $0.001\%.\ s^{-1}$ were applied in the present investigation (thereby spanning an industry relevant range of loading rates). An improved prediction of long term stress relaxation is one of the main advantages that the modified strain-decomposition used here has over the more commonly implemented $\varepsilon = \varepsilon_e + \varepsilon_{vp}$. In order to reduce the amount of required experiential time for anhysteretic type tests, anhysteretic loading cycles (i.e. those with intermediate strain hold periods) were applied for 2 cycle durations at 50 cycle intervals. Intermediate cycles were of a fully reversed "sawtooth" variety (see the following section for an explanation of this) with identical loading rate and loading limit values (compared to the anhysteretic) cycles. That is to say, tests were initiated by 2 anhysteretic waveforms, followed by 48 sawtooth waveforms, followed by 2 anhysteretic waveforms, and so on. In doing this, anhysteretic behaviour could be readily observed at several accumulated plastic strain levels without requiring length experimental procedures.

Standard cyclic test results (fully reversed loading with or without short duration hold periods at peak loads) are primarily used in the present work for validation of the developed material model and optimised material constants. Simple fully reversed cycles with no hold periods are referred to as "sawtooth" type waveforms and were conducted at a constant strain rate (namely $0.1\%.\ s^{-1}$) for strain ranges of $\pm$ 0.5%, $\pm$ 0.4%, and $\pm$ 0.25%. "Dwell" type waveforms were applied for the same strain rate and for limits of $\pm$ 0.5%, wherein a hold period of $120\ s$ is introduced at the maximum load (0.5%). Schematic representations of these waveforms are given in Fig. 2.

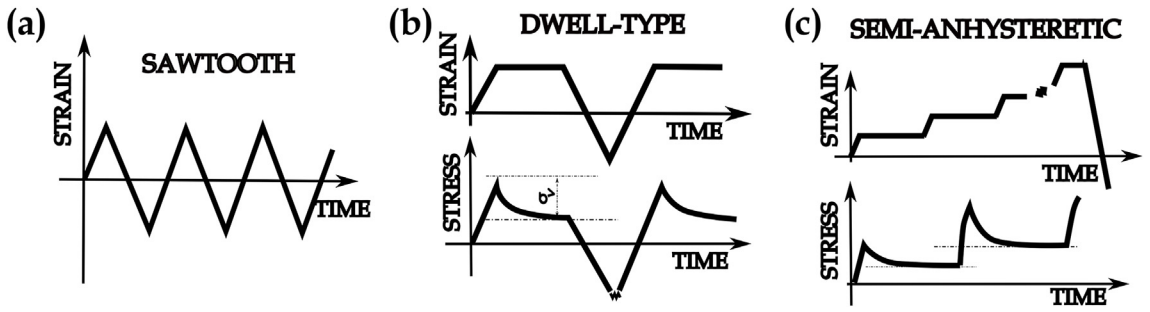

Fig. 2. Strain controlled LCF loading procedures applied on 9–12% Cr steel. (a–b) "Sawtooth" and "Dwell" type waveform schematics (in all cases loaded at $0.1\%.\ s^{-1}$); (c) Semi-anhysteretic waveforms, containing $2.5hr$ strain hold periods at 0.1%, 0.2%, 0.3%, 0.4%, and 0.5% total strain. Strain rates of $0.1\%.\ s^{-1}$, $0.01\%.\ s^{-1}$, and $0.001\%.\ s^{-1}$ have been applied in the present work.

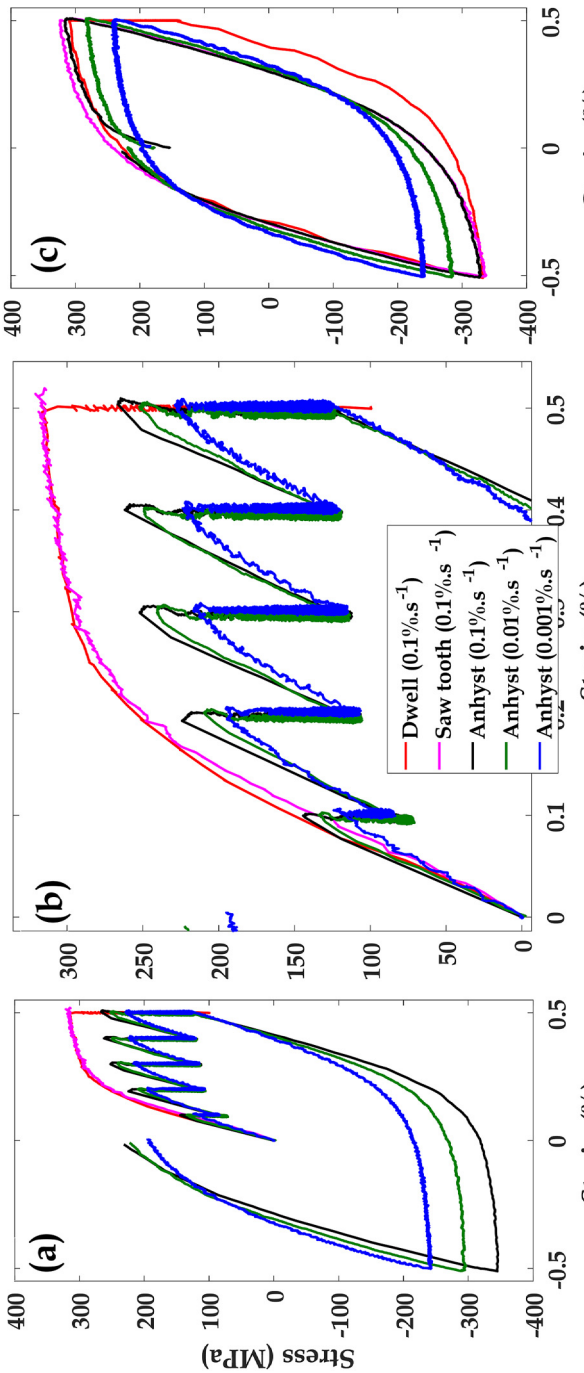

Fig. 3. A comparison of experimental results for Semi-anhysteretic ("Anhyst"), sawtooth and dwell type loading waveforms. Note that 3 strain rates were applied to the Semi-anhysteretic test (namely 0.1%. s^{-1}, 0.01%. s^{-1}, and 0.001%. s^{-1}) and 1 strain rate was used for sawtooth and dwell test (0.1%. s^{-1}), see Fig. 2. Figures are arranged to show (a–b) material response during the cyclic and monotonic loading region and first load reversal, (c) material response during the third loading cycle.

2.2. Experimental observations

By comparing several aspects of the experimental results (and noting obvious differences between the three waveform types) the motivation for incorporating a more accurate representation of viscous effects (i.e. and viscoplastic behaviour) can be made clear. Such a comparison can be seen in Fig. 3, with results presented for anhysteretic, sawtooth and dwell type waveforms.

Initial attention will be paid to the simpler case of a fully reversed cycle with no stress relaxation (strain hold) period (see. Fig. 3c). Comparing "Sawtooth" and "Anhyst" it is obvious that there is a good level of accordance between the material response for tests conducted at identical strain rates (namely 0.1%. s^{-1}). Furthermore, it can be seen that there is also agreement between the "Dwell" tensile data and these results. From these observations it can be suggested that the accumulation of plastic (or perhaps more aptly, inelastic) strain during stress relaxation periods (either during the initial anhysteretic waveforms or at the load reversal in dwell type tests) does not have a significant effect on the hardening behaviour. We may therefore (at least initially) consider isotropic hardening in isolation; with an appropriate description of viscous stress it is expected that hardening can be described by common phenomenological models.

The effects of viscous stress relaxation can be highlighted even more clearly in Fig. 3a–b, where a marked difference is observed between peak stresses in the tensile loading branch. This is despite almost no difference being observed a few cycles later (in Fig. 3c, suggesting that this observation is not due to aleatory uncertainty). The inclusion of strain hold periods allows for the relaxation of viscous stress during monotonic loading, therefore the magnitude of viscous stress at the load reversal in the "Anhyst" curves is significantly less than in the "Dwell" curves. The difference in stresses prior to hold period application in the "Anhyst" curves bears out this point further (in slower loading rate tests the viscous stress has a greater amount of time to relax away during the application of load).

Another important observation can be seen in the first stress relaxation period in Fig. 3b. (at 0.1%). It is noted that stresses relax to approximately 70 *MPa*; a value well below what would usually considered to be the yield stress of P91 at 600 °*C* (circa 170 *MPa*). This observation cannot be accommodated in usual viscoplastic strain decompositions ($\varepsilon = \varepsilon_e + \varepsilon_{vp}$) without imposing a very low initial yield surface size (this has often been observed in the literature). It has been remarked on several occasions that the power flow rule is ineffective as laboratory tests are typically conducted using loading rates that are several orders of magnitude greater than those experienced by in service components (see Barrett et al. (2013)). Even with the application of a more sophisticated flow rule (a hyperbolic sine function, for example) however stresses may not relax below the yield surface (if the viscoplastic formulation is applied). Indeed, it is foreseeable that "plastic" viscous stress contributions will be overestimated if contributions are neglected entirely (as has been the case in most of the published literature relating to P91).

A final observation can be extracted from the evolution of "Sawtooth" hysteresis loops with regard to the number of cycles in Fig. 4. It can be noted that cyclic response of 91 steel exhibits an obvious cyclic softening behaviour. Generally speaking, the cyclic softening continues to evolve during the whole fatigue life. It increases markedly at the very beginning of loading and seems to soften slowly but never before a few hundred cycles. Finally, the cyclic softening accelerates at the last stage of loading before the macroscopic failure of the material (see Saad et al. (2013)). The trend of cyclic softening is observed to be highly affected by the applied strain amplitude. A decrease of 58, 78 and 132 MPa in the maximum stress values from the first to the half-time life are observed for 0.25%, 0.4% and 0.5%, respectively.

3. Constitutive model

In the GSM formalism, any material behaviour can be defined by two potentials: thermodynamic potential Ψ and dissipation potential Φ. The thermodynamic potential, classically considered as Helmholtz free energy, is a state function. Its partial derivatives with respect to the state variables are the so-called state equations, i.e. relations between the state variables and their conjugated variables. The thermomechanical properties of equilibrium states can be completely described using this thermodynamic potential. Irreversibilities associated with deformation processes are introduced via the dissipation potential, which is a function of the state variable rates. The partial derivatives of this dissipation potential with respect to the state variable rates give the so-called evolution (or complementary) equations, i.e. relations between the state variable vector rates and its associated vector of thermodynamic forces.

3.1. Free energy and conjugate variables

The difficulty of the constitutive model can be directly related to the choice of the thermodynamic potential Ψ and the number of assumed internal state variables. In this paper, the material undergoes five processes during the investigated mechanical solicitations. These include prior elasticity, (short/medium/long) term viscoelasticity effects, and non linear viscoplasticity. The short-term viscoelasticity is characterized by the influence of loading rate on the initial stiffness, whereas the medium and long term viscoelasticities are highlighted by the time dependent response to the mechanical loading at long-term time scales. The motivation for the inclusion of non linear viscoplasticity is experimental evidence for irreversible strain accumulation above the stress threshold and also for the observed cyclic softening and hardening. Thus the thermodynamic potential can be decomposed into a set of five components, namely Ψ_e, $\{\Psi_{vj}\}_{j=1,3}$, and Ψ_{vp} (representing prior elasticity, viscoelasticity, and viscoplasticity, respectively). The

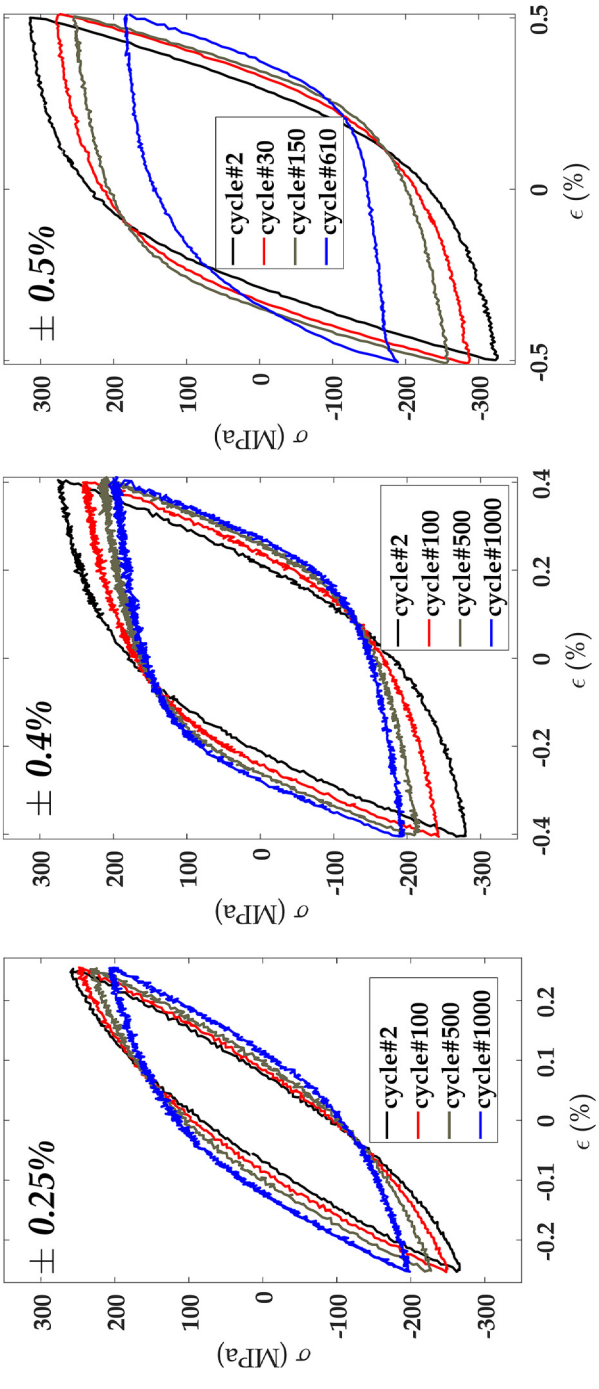

Fig. 4. Stress vs strain responses at three strain amplitudes (0.25%, 0.4% and 0.5%) from zero-hold time tests carried out at 600°C with a loading strain rate of 0.1%. s^{-1}.

decomposition of the thermodynamic potential into the elastic and viscoplastic components for elastic-viscoplastic materials is well established (see Chaboche (2008)). Note that the novelty in the model presented here is the addition of three components of viscoelasticity, with this inclusion being motivated by the following question: *Can stresses, if given enough time under constant load conditions, relax below the cyclic yield stress (instantaneous yield locus size) of the material and, if this is the case, will the unloading behaviour remain elastic after relaxation?*. Experimental observations discussed previously seem to confirm that stresses will indeed relax below the yield. On a related note, it is important to realise that the presented formulation allows for the total relaxation of the material (i.e. to a zero stress). In a real material, it is conceivable that some micro-structural obstacle will prevent this, thereby giving rise to a non-zero stress. Such effects were not observed for the long dwell times considered here and, as they do not bear a great deal of significance for the proposed model application, are neglected from consideration. Based on the experimental observations extracted from strain controlled anhysteretic tests obtained at different strain rates (see Subsec. 2.2), the above assumption seems to be valid. Thus, we assume the specific free energy can be decomposed as:

$$\Psi := \Psi_e(\underline{\underline{\varepsilon}}_e) + \sum_{j=1}^{3} \Psi_{vj}\left(\underline{\underline{\varepsilon}}_{vj}\right) + \Psi_{vp}\left(\underline{\underline{\varepsilon}}_{vp}, \underline{\underline{\alpha}}, r\right), \tag{1}$$

where $\underline{\underline{\varepsilon}}_e$, $\left\{\underline{\underline{\varepsilon}}_{vj}\right\}_{j=1,3}$ and $\underline{\underline{\varepsilon}}_{vp}$ are, respectively, the elastic, viscoelastic and viscoplastic strain tensors. The term $\underline{\underline{\alpha}}$ stands for the kinematic hardening variable and r the isotropic hardening variable. Note that r is no longer exactly the viscoplastic multiplier λ (alternatively accumulated plastic strain p), however when recovery effects are small this internal variable is identifiable as λ (see Chaboche (2008)). It should be mentioned that one can decompose the thermodynamic potential into its components and yet capture the coupling between different processes. In a stricter sense, a realistic model should take into account temperature as an observable variable to model the thermomechanical couplings and carry out anisothermal analyses. These aspects considered to be outside of the scope of the present work, however interested readers are directed to the author's previous work (Benaarbia et al. (2016)).

At a reference temperature T_o, the 3D constitutive model is associated with the following Helmholtz free energy potential Ψ, function of the state variables $\left\{\underline{\underline{\varepsilon}}, \left\{\underline{\underline{\varepsilon}}_{vj}\right\}_{j=1,3}, \underline{\underline{\varepsilon}}_{vp}, \underline{\underline{\alpha}}, r\right\}$:

$$\Psi\left(\underline{\underline{\varepsilon}}, \left\{\underline{\underline{\varepsilon}}_{vj}\right\}_{j=1,3}, \underline{\underline{\varepsilon}}_{vp}, \underline{\underline{\alpha}}, r\right) = \frac{1}{2}\left(\underline{\underline{\varepsilon}} - \sum_{j=1}^{3} \underline{\underline{\varepsilon}}_{vj} - \underline{\underline{\varepsilon}}_{vp}\right) : \mathbb{C}_e : \left(\underline{\underline{\varepsilon}} - \sum_{j=1}^{3} \underline{\underline{\varepsilon}}_{vj} - \underline{\underline{\varepsilon}}_{vp}\right) + \frac{1}{2}\sum_{j=1}^{3} \underline{\underline{\varepsilon}}_{vj} : \mathbb{C}_{vj} : \underline{\underline{\varepsilon}}_{vj} + \frac{2}{9}\sum_{i=1}^{2} c_i J_2^2(\underline{\underline{\alpha}}_i) + \frac{Q_1}{b}(br + \exp(-br)) + \frac{1}{2}Q_2 r^2, \tag{2}$$

where $\mathbb{C}_e$ and $\{\mathbb{C}_{vj}\}_{j=1,3}$ represent the fourth order isotropic elastic and viscous tensors, respectively. In the above expressions, all the second order tensors are symmetric and all of the fourth order tensors have minor and major symmetries. The term J_2 represents the second invariant defined as $J_2(\underline{\underline{x}}) = (3/2\,\underline{\underline{x}}^d : \underline{\underline{x}}^d)^{1/2}$ with $\underline{\underline{x}}^d$ stands for the deviatoric part of $\underline{\underline{x}}$. The symbol : represents the product contracted twice (i.e. $\underline{\underline{x}} : \underline{\underline{x}} = \mathrm{Tr}(x^2)$ where $\mathrm{Tr}(.)$ denotes the trace of a second order tensor. Note that b, Q_1 and Q_2 are the isotropic hardening model constants while $\{c_i\}_{i=1,2}$ the kinematic ones.[1]

The state laws can then be derived from the partial derivatives of the thermodynamic potential as follows:

- The Cauchy stress:

$$\underline{\underline{\sigma}} = \frac{\partial \Psi}{\partial \underline{\underline{\varepsilon}}_e} = \mathbb{C}_e : \left(\underline{\underline{\varepsilon}} - \sum_{j=1}^{3} \underline{\underline{\varepsilon}}_{vj} - \underline{\underline{\varepsilon}}_{vp}\right), \tag{3}$$

- The conjugate variable of $\underline{\underline{\varepsilon}}_{vj}$:

$$\underline{\underline{\chi}}_{vj} = \frac{\partial \Psi}{\partial \underline{\underline{\varepsilon}}_{vj}} = -\underline{\underline{\sigma}} + \mathbb{C}_{vj} : \underline{\underline{\varepsilon}}_{vj}, \quad \text{with } j = 1,3 \tag{4}$$

- The conjugate variable of $\underline{\underline{\varepsilon}}_{vp}$:

$$\underline{\underline{\chi}}_{vp} = \frac{\partial \Psi}{\partial \underline{\underline{\varepsilon}}_{vp}} = -\underline{\underline{\sigma}}, \tag{5}$$

[1] The Chaboche type kinematic hardening rule with 2 back stress contributions $\{\underline{\underline{X}}_i\}_{i=1,2}$ is adopted in the present work (see. Chaboche and Rousselier (1983)).

- The elementary backstress tensors:

$$\underline{\underline{X}}_i = \frac{\partial \Psi}{\partial \underline{\underline{\alpha}}_i} = \frac{2}{3} c_i \underline{\underline{\alpha}}_i, \quad \text{with } i = 1,2 \tag{6}$$

- The isotropic hardening variable:

$$R = \frac{\partial \Psi}{\partial r} = Q_1(1 - \exp(-br)) + Q_2 r. \tag{7}$$

3.2. Dissipation potential and thermodynamic forces

All of the state equations derived above describe the properties of the material in an equilibrium state. Irreversibilities are taken into account by means of complementary laws. Within GSM theory, the evolution laws are deduced from a convex dissipation potential Φ function of the state variable rates $\left\{\dot{\underline{\varepsilon}}, \left\{\dot{\underline{\varepsilon}}_{vj}\right\}_{j=1,2,3}, \dot{\underline{\varepsilon}}_{vp}, \{\dot{\underline{\alpha}}_i\}_{i=1,2}, \dot{r};\ T_o,\ r\right\}$. This potential is (by construction) positive and minimal at $\dot{\underline{\varepsilon}} = \left\{\dot{\underline{\varepsilon}}_{vj}\right\}_{j=1,2,3} = \dot{\underline{\varepsilon}}_{vp} = \{\dot{\underline{\alpha}}_i\}_{i=1,2} = \dot{r} = 0$. The mathematical assumptions taken in the construction of the dissipation potential ensures that the second principle of thermodynamics is satisfied (i.e. a total dissipation non-negative as stipulated by the Clausius-Duhem inequality). In the viscoplasticity framework, it is more convenient to define a dual dissipation potential Φ^* function of thermodynamic forces $\underline{\sigma}_{ir}$ [2], $\left\{\underline{\underline{\mathscr{T}}}_{vj}\right\}_{j=1,2,3}$, $\underline{\underline{\mathscr{T}}}_{vp}$, $\{-\underline{\underline{X}}_i\}_{i=1,2}$, and $-R$. This potential can be obtained using the Legendre-Fenchel transform of Φ (see Halphen and Nguyen (1975)). Thus, the following expression is adopted:

$$\Phi^*\left(\underline{\sigma}, \left\{\underline{\underline{\mathscr{T}}}_{vj}\right\}_{j=1,2,3}, \underline{\underline{\mathscr{T}}}_{vp}, \{-\underline{\underline{X}}_i\}_{i=1,2}, -R;\ T_o,\ r\right) := \int \dot{\varepsilon}_{o_{vp}} \left[sinh\left(\frac{f(\underline{\sigma}, \underline{\underline{X}}, \underline{\underline{\alpha}}, R;\ T_o,\ r)}{K_{vp}}\right)\right]^{m_{vp}} df + \frac{1}{2}\sum_{j=1}^{3} \underline{\underline{\mathscr{T}}}_{vj} : \mathbb{D}_{vj}^{-1} : \underline{\underline{\mathscr{T}}}_{vj} + \Phi_r^*. \tag{8}$$

Parameters $\dot{\varepsilon}_{o_{vp}}$, K_{vp} and m_{vp} introduced in the hyperbolic sine law are, respectively, the initial viscoplastic strain rate, viscoplastic resistance coefficient and hardening exponent. $\underline{\underline{X}}$ stands for the sum of the 2 elementary back stresses $\{\underline{\underline{X}}_i\}_{i=1,2}$, while $\{\mathbb{D}_{vj}\}_{j=1,3}$ represents the fourth order isotropic viscosity tensors. Φ_r^* is a recovery potential which is assumed in the following to be equal to zero (i.e. the flux variable $\dot{r} = -\partial\Phi^*/\partial R$ is identified with the viscoplastic multiplier rate $\dot{\lambda}$, see Eq. (13)).

The studied material is assumed to be isotropic and the yield criteria to be independent of the hydrostatic pressure (only depends on the deviatoric components of stresses). Thus, the Von Mises yield criterion, function of the invariants of the deviatoric stresses, is considered as follows (see Lemaitre and Chaboche (2000)):

$$f(\underline{\sigma}, \underline{\underline{X}}, \underline{\underline{\alpha}}, R;\ T_o, \lambda) = \mathrm{J}_2(\underline{\sigma} - \underline{\underline{X}}) - R - \sigma_y + \frac{1}{2}\sum_{i=1}^{2} \frac{\gamma_i(\lambda)}{c_i} \mathrm{J}_2^2(\underline{\underline{X}}_i) - \frac{2}{9}\sum_{i=1}^{2} c_i \gamma_i(\lambda) \mathrm{J}_2^2(\underline{\underline{\alpha}}_i), \tag{9}$$

where σ_y defines the yield stress while $\{\gamma_i\}_{i=1,2}$ stand for kinematic hardening model constants.

The complementary equations can then be derived from the dual dissipation potential as follows:

- The viscous strain rates:

$$\dot{\underline{\varepsilon}}_{vj} = \frac{\partial \Phi^*}{\partial \underline{\underline{\mathscr{T}}}_{vj}} = \mathbb{D}_{vj}^{-1} : \underline{\underline{\mathscr{T}}}_{vj}, \quad \text{with } j = 1,3 \tag{10}$$

- The viscoplastic strain rate:

$$\dot{\underline{\varepsilon}}_{vp} = \frac{\partial \Phi^*}{\partial \underline{\underline{\mathscr{T}}}_{vp}} = -\frac{\partial \Phi^*}{\partial f}\frac{\partial f}{\partial \chi_{vp}} = \underbrace{\dot{\varepsilon}_{o_{vp}} \left[sinh\left(\frac{f(\underline{\sigma}, \underline{\underline{X}}, \underline{\underline{\alpha}}, R;\ T_o, \lambda)}{K_{vp}}\right)\right]^{m_{vp}}}_{\dot{\lambda}\text{: viscoplastic multiplier rate}} \underline{\underline{\mathbb{N}}}_{vp}, \tag{11}$$

[2] In this model, the irreversible component of stress $\underline{\sigma}_{ir}$ is equal to zero and the total stress tensor $\underline{\sigma}$ is identical with its reversible component.

where $\underline{\underline{\mathbb{N}}}_{vp}$ denotes the viscoplastic flow direction (the partial derivative of the yield function with respect to the total stress tensor).

- The rate of the internal variables $\underline{\underline{\alpha}}_i$:

$$\dot{\underline{\underline{\alpha}}}_i = -\frac{\partial \Phi^*}{\partial \underline{\underline{X}}_i} = -\frac{\partial \Phi^*}{\partial f}\frac{\partial f}{\partial \underline{\underline{X}}_i} = \dot{\underline{\underline{\varepsilon}}}_{vp} - \gamma_i \underline{\underline{\alpha}}_i \dot{\lambda}, \quad \text{with } i = 1,2. \tag{12}$$

- The rate of the internal variable r:

$$\dot{r} = -\frac{\partial \Phi^*}{\partial R} = -\frac{\partial \Phi^*}{\partial f}\frac{\partial f}{\partial R} = \dot{\lambda}. \tag{13}$$

The evolution rule of $\underline{\underline{\alpha}}_i$ introduces an evanescent strain memory to capture the Bauschinger effects observed at the experimental hysteresis loops. The substitution of the back stress tensor expression $\underline{\underline{X}}_i$ (Eq. (6)) into the internal variable rate expression $\dot{\underline{\underline{\alpha}}}_i$ (Eq. (12)), enables to have the following isothermal kinematic hardening stress evolution rule (see Lemaitre and Chaboche (2000)):

$$\dot{\underline{\underline{X}}}_i = \frac{2}{3} c_i \dot{\underline{\underline{\varepsilon}}}_{vp} - \gamma_i \dot{\lambda} \underline{\underline{X}}_i; \quad \text{with } i = 1,2. \tag{14}$$

After time derivation of the drag stress R in (Eq. (7)), one can obtain the following evolution rule of isotropic hardening stress:

$$\dot{R} = Q_2(1 + br)\dot{\lambda} + b(Q_1 - R)\dot{\lambda}. \tag{15}$$

In summary, the proposed viscoelastic-viscoplastic constitutive model can be described by the set of constitutive equations given in Table 1.

4. Initial parameter values identification

4.1. Uniaxial formulation of constitutive equations

The calibration and validation of the proposed model is mainly based on the one-dimensional formulation of the constitutive model with the assumption of an initially isotropic and homogeneous material. A convenient rheological representation of the one-dimensional scheme is illustrated in Fig. 5. In order to give confidence in the foregoing theory with a physically based structure, we split the schema into 5 components: elastic, 3 viscoelastic and viscoplastic. Therefore, the rheological model contains springs with linear stiffnesses (E_o and $\{E_{vj}\}_{j=1,2,3}$), damping branches with linear viscosities ($\{\eta_{vj}\}_{j=1,2,3}$) and a nonlinear friction element with plastic hardening (c_i and γ_i with $i = 1,2$; Q_1, Q_2 and b) coupled with a nonlinear damping branch (K_{vp} and m_{vp}). From a physical point of view, the current rheological model is thermodynamically consistent and compatible with the second principle of thermodynamics. The relaxation (characteristic) times for the Kelvin-Voigt viscoelastic elements are defined as $\tau_{vj} = \eta_{vj}/E_{vj}$ with $j = 1,2,3$. The Kelvin-Voigt elements are used to model the experimentally observed viscoelasticity observed at different time-scales (we can discuss about short, medium and long term viscoelasticities). Whereas, the viscoplastic element is devoted to numerically capture irrecoverable mechanisms such as viscoplasticity as well as nonlinear isotropic and kinematic hardening.

Following the GSM theory, the conjugate variables are minus-identical with the thermodynamic forces. This leads us to the following uniaxial simplification of the yield criterion and the equations of flow and hardening:

- The Cauchy stress:

$$\sigma = E_o(\varepsilon - \varepsilon_{v1} - \varepsilon_{v2} - \varepsilon_{v3} - \varepsilon_{vp}). \tag{16}$$

Table 1
Summary set of the viscoelastic-viscoplastic constitutive model.

• Total strain decomposition:	$\underline{\underline{\varepsilon}} = \underline{\underline{\varepsilon}}_e + \underline{\underline{\varepsilon}}_{v1} + \underline{\underline{\varepsilon}}_{v2} + \underline{\underline{\varepsilon}}_{v3} + \underline{\underline{\varepsilon}}_{vp}$.
• Rate of viscoelastic strains:	$\dot{\underline{\underline{\varepsilon}}}_{vj} = \underline{\underline{\mathbb{D}}}_{vj}^{-1} : \underline{\underline{\dot{\mathscr{T}}}}_{vj}, \quad \text{with } j = 1,3.$
• Yield function:	$f(\underline{\underline{\sigma}}, \underline{\underline{X}}, \underline{\underline{\alpha}}, R;\ T_o, \lambda) = \mathrm{J}_2(\underline{\underline{\sigma}} - \sum_{i=1}^{2} \underline{\underline{X}}_i) - R - \sigma_y + \frac{1}{2}\sum_{i=1}^{2} \frac{\gamma_i(\lambda)}{c_i}\mathrm{J}_2^2(\underline{\underline{X}}_i) - \frac{2}{9}\sum_{i=1}^{2} c_i\gamma_i(\lambda)\mathrm{J}_2^2(\underline{\underline{\alpha}}_i)$.
• Viscoplastic strain rate:	$\dot{\underline{\underline{\varepsilon}}}_{vp} = \dot{\varepsilon}_{o_{vp}}\left[sinh\left(\frac{f(\underline{\underline{\sigma}}, \underline{\underline{X}}, \underline{\underline{\alpha}}, R;\ T_o, \lambda)}{K_{vp}}\right)\right]^{m_{vp}} \underline{\underline{\mathbb{N}}}_{vp}$.
• Kinematic hardening rule:	$\underline{\underline{X}} = \sum_{i=1}^{2} \underline{\underline{X}}_i; \quad \dot{\underline{\underline{X}}}_i = \frac{2}{3} c_i \dot{\underline{\underline{\varepsilon}}}_{vp} - \gamma_i \dot{\lambda} \underline{\underline{X}}_i$.
• Isotropic hardening rule:	$\dot{R} = Q_2(1 + br)\dot{\lambda} + b(Q_1 - R)\dot{\lambda}$.

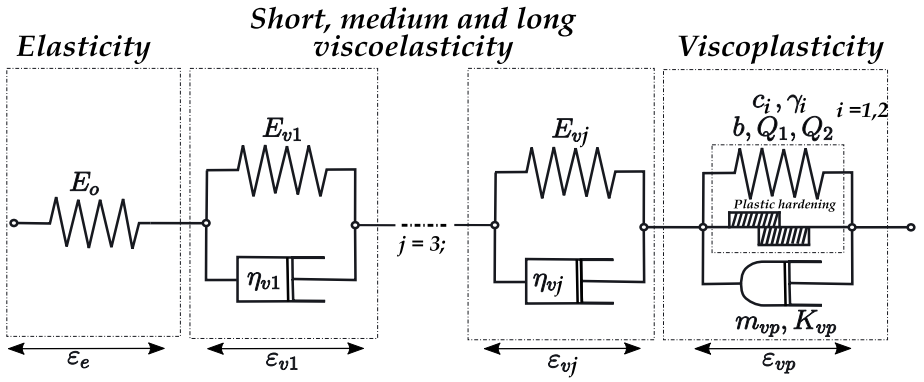

Fig. 5. 1D-rheological scheme of the proposed constitutive model.

- The viscoelastic strain rate:

$$\dot{\varepsilon}_{vj} = \eta_{vj}^{-1}(\sigma - E_{vj}\varepsilon_{vj}), \text{ with } j = 1,2,3. \tag{17}$$

- The viscoplastic strain rate:

$$\dot{\varepsilon}_{vp} = \dot{\varepsilon}_{o_{vp}}[sinh(f/K_{vp})]^{m_{vp}}\text{sign}(\sigma - X). \tag{18}$$

- The yield function:

$$f = |\sigma - X| - R - \sigma_y. \tag{19}$$

- The backstress decomposition:

$$X = X_1 + X_2. \tag{20}$$

- The rate of backstress:

$$\dot{X}_i = c_i\dot{\varepsilon}_{vp} - \gamma_i X_i|\dot{\varepsilon}_{vp}|, \text{ with } i = 1,2. \tag{21}$$

- The rate of drag stress:

$$\dot{R} = Q_2(1 + br)|\dot{\varepsilon}_{vp}| + b(Q_1 - R)|\dot{\varepsilon}_{vp}|. \tag{22}$$

4.2. 1D solution computation and material constant optimisation

The viscoelastic-viscoplastic model presented here uses a total of 18 material parameters to describe the cyclic response of P91 steel for uniaxial loading conditions. These parameters are to be determined through an optimisation procedure (i.e. by fitting the model to experimental results, such that a locally minimum value of some objective function is obtained). A problem arises however; the viscoelastic and viscoplastic mechanisms are highly coupled and it is likely that effects attributed to one mechanism are, in reality, due to another (for example, viscous stress relaxation may be misinterpreted as the evolution of back stress when experimental results for a single loading rate are viewed in isolation). This problem is present for simple viscoplastic models and is only compounded for the more complex model used here. In order to address this issue and determine representative material constants a step by step approach is implemented here, with viscoelastic material properties estimated first (by neglecting viscoplastic effects) and then the remaining kinematic/viscoplastic materiel parameters estimated afterwards (with estimated viscoelastic contributions accounted for). A final optimisation procedure, which attempts to fine tune all 18 material constants to properly represent the highly

coupled phenomena, is ultimately performed using these estimates as a starting point. A general optimisation methodology is implemented at each stage in this process and will now be described (methods that produce estimates of the viscoelastic and viscoplastic material parameters are discussed in subsequent sections).

The optimisation of the material constants described in Eqs. (16-22) and the validation of these material constants against additional experimental data requires that the system of ODEs in Eqs. (16-22) be solved. For 1D simulations, the ODEs can be readily solved in MATLAB. This can be achieved implicitly for situations where deformation is entirely known (see the following section for more details). The full system of ODEs was solved explicitly using a Dormand-Prince ($4^{th}/5^{th}$ order Runge-Kutta) algorithm (ODE45 in MATLAB). In all cases, model approximations were generated using idealised (i.e. without noise) strain loading waveforms which were calculated based on the intended control parameters (i.e. strain rate and strain limits), thereby eliminating the effects of noise in the experimental load waveform.

A Levenberg-Marquardt algorithm (LSQNONLIN in MATLAB) was used for the purposes of optimisation in both viscoelastic and viscoplastic cases. A single objective function (comparing experiential and predicted stress magnitudes at the i^{th} instant for the j^{th} data set, $\sigma_{i,j}^{exp}$ and $\sigma_{i,j}^{num}$, respectively) was applied to judge "goodness of fit" for each of the experimental data sets (j = 1,2,3 here, representing the three loading rates applied to anhysteretic waveforms in the present work). A cost function was evaluated (at each optimisation iteration) by combining objective function values for each of the data sets (appropriately scaled to ensure similar contributions from test result sets with significantly different stress magnitudes) to be considered in the optimisation procedure. The total cost function $\mathcal{F}_c$ that the optimisation procedure acts to minimize can therefore be represented by the expression shown below:

$$\mathcal{F}_c = \sum_{j=1}^{3}\sum_{i=1}^{n_f} \Gamma_j(\sigma_{i,j}^{exp} - \sigma_{i,j}^{num})^2. \tag{23}$$

In Eq. (23) the objective function is summed of j data sets (or experiments, here the three anhysteretic results) and $\sigma_{i,j}^{exp}$ & $\sigma_{i,j}^{num}$ are the experimental and numerical stress values (for the i^{th} data point in the j^{th} data set), respectively. Γ_j is a weighting function that normalises contributions from the j^{th} test and n_f is the number of data points (evenly) sampled from the particular data set. Numerical results were interpolated where necessary in order to evaluate the objective function at identical time instants.

4.3. Determination of initial viscoelastic coefficients

Determination of material parameters was achieved by optimising the trial model parameters against the initial loading branch of the anhysteretic waveform (i.e. the loading up to and including the first strain hold period), as, during the initial loading region and for stresses below yielding (σ_y in Eq. (19)), it may be assumed that $\varepsilon_{vp} = 0$. In neglecting the viscoplastic strain contribution the governing equations are greatly simplified. Strain magnitudes in the spring and Kelvin-Voigt elements (see Fig. 5) may therefore be solved for implicitly (thereby eliminating the need to invoke MATLAB's ODE45 function during the first optimisation procedure). A simplified 2 Kelvin-Voigt element model was initially implemented (for the description of deformation prior to plasticity) so that orders of magnitude could be determined for the corresponding material parameters. Initial estimates for the material parameters (which were needed as a starting point for the first optimisation procedure) were made by taking a typical value for Young's modulus (136 GPa) for P91 at 600 ^oC, assuming that this was a suitable approximation for the spring constant values (E_o, E_{v1}, and E_{v2}), and applying expected Kelvin-Voigt element characteristic time values (10 s and 100 s) so that corresponding damping coefficients could be calculated (η_{v1} and η_{v2}). Sufficiently large bounds were placed on each of the coefficients during optimisation (equivalent to plus and minus three orders of magnitude for the spring coefficients) so that the solution was not overly constrained by these coarse approximations. Note that characteristic time values were chosen in order to describe so-called short and medium term behaviour. For completeness, the implicit scheme for the solution is presented as follows:

$$\begin{cases} \varepsilon_{v1}^{n+1} &= \varrho((1-\varkappa)\Delta t E_o\, \varepsilon^{n+1} + \eta_{v1}\varepsilon_{v1}^{n} - \varkappa\eta_{v2}\varepsilon_{v2}^{n})\Delta t^{-1}, \\ \varepsilon_{v2}^{n+1} &= E_o^{-1}(\varkappa\Delta t E_o\varepsilon^{n+1} - \varkappa t E_o\varepsilon_{v1}^{n} + \varkappa\eta_{v2}\varepsilon_{v2}^{n})\Delta t^{-1}, \\ \sigma^{n+1} &= E_o(\varepsilon^{n+1} - \varepsilon_{v1}^{n+1} - \varepsilon_{v2}^{n+1}), \\ with \quad \varkappa &= E_o(E_{v2} + \Delta t^{-1}\eta_{v2} + E_o)^{-1}, \\ \varrho &= (1-\varkappa)E_o + E_{v1} + \Delta t^{-1}\eta_{v1}. \end{cases} \tag{24}$$

Table 2
A summary of the initial material constants (determined from the monotonic anhysteretic data).

Mechanical feature	Model parameter	Symbol	Unit	Value
Elasticity	Young Modulus	E_o	GPa	131.74
Short-term viscoelasticity	Viscosity	η_{v1}	GPa.s	3400.04
	Stiffness modulus	E_{v1}	GPa	409.98
	Characteristic time	τ_{v1}	s	8.29
medium-term viscoelasticity	Viscosity	η_{v2}	GPa.s	76123.21
	Stiffness modulus	E_{v2}	GPa	331.96
	Characteristic time	τ_{v2}	s	229.31

Related material constants (namely E_o, E_{v1}, η_{v1}, E_{v2}, and η_{v2}) were fitted to the monotonic data (i.e. until the end of the first hold period) from the anhysteretic waveform. In this way, total strain never exceeds 0.1% and the material behaviour was judged to be only. A summary of the material parameters determined by the optimisation method discussed above are given in Table 2, with the corresponding material response predictions given in Fig. 6. It is noted that with the simple two element model strain rate dependency in the (apparent) elastic region can be fully predicted as shown in Fig. 6a. Asymptotic behaviour is also estimated in the first strain hold (stress relaxation) region through consistent estimates of the long term stress relaxation rate (see Fig. 6b).

4.4. Determination of long-term viscoelastic-viscoplastic coefficients

Approximate orders of magnitude for parameters in the 2 Kelvin-Voigt elements were determined in the previous section (see Table 2, based on optimisations against the first strain hold period in the anhysteretic data). These material parameters can be considered to represent short and medium term effects (i.e. acting with characteristic times of 8.3 and 230.0 s for both components ε_{v1} and ε_{v2}, respectively) and were taken to be initial estimates of these parameters in the full (viscoplastic) optimisation problem. To include long term viscoelastic effects a third Kelvin-Voigt element was added to the model. Parameters related to this term (E_{v3} and η_{v3}) were optimised along with all other parameters in the final optimisation procedure, however initial estimates were of course required. An approximate value for the additional spring coefficient (E_{v3}) was as the mean values of corresponding ε_{v1} and ε_{v2} coefficients. The estimate of E_{v3} was then used in turn to approximate η_{v3} by assuming a long term representative characteristic time for ε_{v3} (taken to be $10^5\ s$). Initial material constant estimates (along with upper and lower bounds) are first determined. Optimised material parameters (along with initial estimates and upper/lower bounds) are given in Table 3; readers may note that the concept of short, medium, and long term components is illustrated by these results.

Initial estimates for the remaining 11 viscoplastic related material parameters were determined by neglecting the viscous effects and applying the well known Cottrell stress partitioning method (see Cottrell (1953); Fournier et al. (2006)). In the interest of space only a brief discussion is given here. The stress partition method can be illustrated through Fig. 7 (note that in this figure i subscripts denote quantities related to the i^{th} cycle, with t and c superscripts indicating tensile and compressive quantities, respectively). In short, the method allows the yield locus size and location to be determined (on the loading axis) for each loading cycle. With this information in hand estimates of the thermodynamic conjugate variables related to hardening (R and X) may be made and related to increments in plastic strain. Approximations of corresponding evolution equations may be fitted to these results in order to estimate the relevant material parameters.

Using the lowest stain rate experimental data (for which the assumption of negligible viscosity is most applicable due to the significant amount of time for stresses to relax during load application), the onset of so-called non-linearity (what may be most readily called yielding) for each cycle can be estimated by an incremental linear regression procedure (σ_i^{t-y} and σ_i^{c-y} for tensile and compressive loading branches, respectively, in Fig. 7). For fully reversed test profiles (or more specifically, where an appreciable amount of plasticity is accumulated on the application both tensile and compressive loads), ascertaining the onset of non-linearity defines a yield locus (note that some none linearity related to viscous effects may be observed at load reversal, thereby giving rise to σ_i^{t-1} and σ_i^{c-1} in Fig. 7. Note that defining σ_i^{t-1} for the first loading cycle indicates an appropriate value for the cyclic yield stress parameter σ_y. It has been observed in previous optimisation exercises that the value of σ_y will be reduced during the procedure (thereby artificially placing a greater emphasis on viscoplastic mechanisms), resulting in an un-realistic final value. To guard against this, tight bounds have been placed on σ_y ($\pm\ 5MPa$), related to the scatter values determined from different data sets), thereby ensuring σ_y remains at a sensible level and viscoelastic and viscoplastic mechanisms are appropriately represented.

In the viscoplastic strain decomposition viscous effects are only considered after yielding, therefore the placement of a yield locus completely defines the conjugate variables X and R (by the centre and size of the yield locus, respectively). In the case of R this

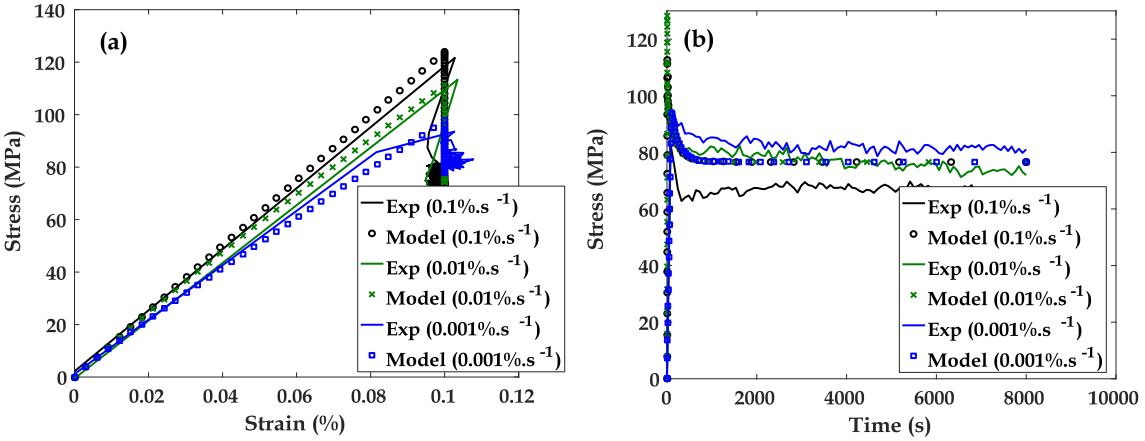

Fig. 6. Partial optimisation results (used for determination of material constants), showing a). the $\sigma - \varepsilon$ response predicted by the model during the initial loading branch, b). the $\sigma - t$ response of the material (verifying the prediction of stress relaxation in an "elastic" region).

Table 3
A summary of the viscoelastic-viscoplastic material constants (determined by applying the optimisation procedure to the anhysteretic data). OV, IE, UB and LB are the optimised values, initial estimates, upper and lower bounds, respectively.

Mechanical feature	Model parameter	Symbol	Unit	IE	UB	LB	OV
Elasticity	Initial Young Modulus	E_o	GPa	131.7	10^3	10.0	142.74
	Initial Cyclic Yield Stress	σ_y	MPa	160.0	165.0	155.0	156.72
	Poisson's ratio	ν	–	–	–	–	0.3
Short-term viscoelasticity	Viscosity	η_{v1}	GPa.s	3400.0	10^9	1.0	20720.94
	Stiffness modulus	E_{v1}	GPa	409.9	10^3	10.0	2974.91
	Characteristic time	τ_{v1}	s	–	–	–	6.96
Medium-term viscoelasticity	Viscosity	η_{v2}	GPa.s	76123.2	10^9	1.0	118673.94
	Stiffness modulus	E_{v2}	GPa	331.9	10^3	10.0	324.73
	Characteristic time	τ_{v2}	min	–	–	–	6.09
Long-term viscoelasticity	Viscosity	η_{v3}	GPa.s	3.5×10^7	10^9	1.0	2089095.82
	Stiffness modulus	E_{v3}	GPa	350.0	10^3	10.0	12.45
	Characteristic time	τ_{v3}	h	–	–	–	46.61
Non linear viscosity	Viscoplastic resistance	K_{vp}	MPa	19.2	25.0	5.0	19.20
	Viscous exponent	m_{vp}	–	1.25	10.0	1.0	1.02
	Initial viscous rate	$\dot{\varepsilon}_{o_{vp}}$	s^{-1}	1.34×10^{-6}	3×10^{-6}	1×10^{-7}	2.69×10^{-6}
Kinematic hardening	Hardening modulus 1	c_1	GPa	3.9	100.0	0.0	7.54
	Non linear parameter 1	γ_1	–	109.7	10^4	0.0	68.48
	Hardening modulus 2	c_2	GPa	6.1	100.0	0.0	26.2
	Non linear parameter 2	γ_2	–	154.2	10^4	0.0	1157.80
Isotropic hardening	Asymptotic parameter	Q_1	MPa	− 70.0	− 50.0	− 75.0	− 64.98
	Isotropic exponent	b	–	3.0	3.0	1.5	1.89
	Isotropic parameter	Q_2	MPa	− 3.0	− 2.8	− 5.0	− 4.82

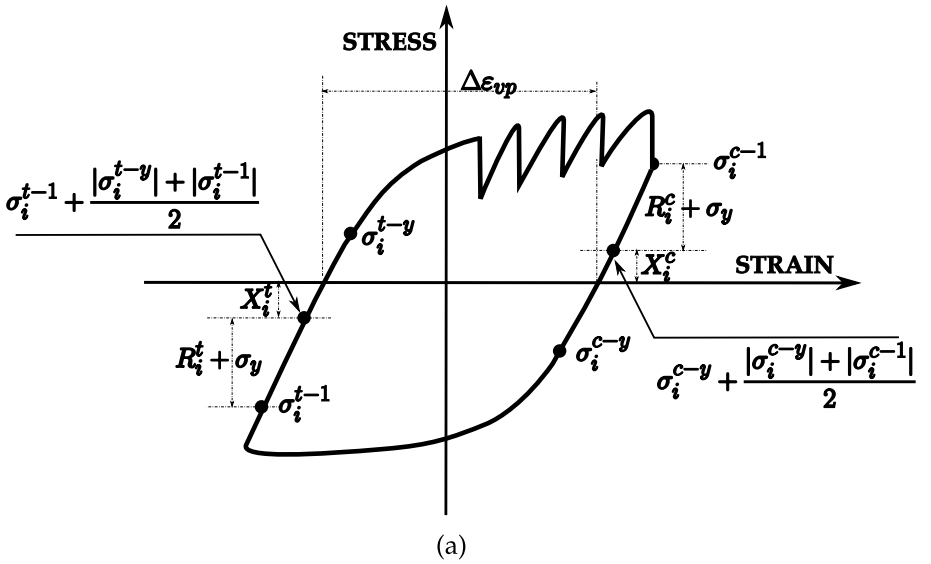

(a)

Fig. 7. A schematic representation of the stress partition method (used to estimate viscoplastic related material parameters).

method fully defines the drag stress evolution (pseudo-saturation), allowing the relevant evolution equation to the fitted to the data and estimates of b, Q_1, and Q_2 to be determined. In Fig. 7, drag stresses for the i^{th} cycle are denoted by R_i^t and R_i^c (for the tensile and compressive loading branches, respectively). Upper and lower bounds for these coefficients may be determined by observing the scatter in the stress partition results.

For back stress X, the stress partition approach defines a saturated value (the upper limit for the ratio c_i/γ_i). Values for X_i^t and X_i^c (the back stresses associated with tensile and compressive loading branches in the i^{th} cycle) can be determined from Fig. 7 by observing the centre of the yield locus for each loading branch (given by $\sigma_i^{t-1} + ((|\sigma_i^{t-y}| + |\sigma_i^{t-1}|)/2)$ in the case of the tensile branch). Using the work of Tong and Vermeulen (2003), individual back stress components may be estimated by assuming the saturation of X during the monotonic loading region of the cyclic data (i.e. the first loading application).

With definitions of the back stress, drag stress and viscoelastic contribution, viscous parameters associated with plasticity (the hyperbolic sine flow rule coefficients) can be estimated by evaluating each of the estimated components during the monotonic loading regions and observing the remaining (unaccounted for) stress component. Initial estimates for each of the material

parameters, along with upper and lower bounds, are first determined. An optimisation procedure was performed to fine tune all material parameters (viscoelastic and viscoplastic) wherein the predicted stress response was fitted to the experientially observed response (as per the description given in previous sections) for the first 200 loading cycles. For clarity, the 1D formulation of the proposed material model given in Eqs. (16-22) is the form that is solved by the MATLAB function ODE45 during the optimisation procedure. Finally, optimised material parameters are presented in Table 3.

5. The cyclic response of P91 steel with optimised parameters

5.1. Semi-anhysteretic cyclic responses

It is clearly important to verify that the fitted viscoelastic-viscoplastic material model is adept at predicting material response due to anhysteretic loading waveforms. To demonstrate this, comparative plots for the three loading rates are presented here. Cycles 1 and 2 (anhysteretic waveforms) are presented in Fig. 8, with hardening response predictions verified in sub figures a) and c) (through the creation of σ-ε plots) and viscous (time dependent) behaviour illustrated in b), d), e) and f). (through σ-t plots). Particular emphasis should be placed on the ability of the model to predict the asymptotic stress relaxation behaviour in the strain hold regions; see Fig. 8 b). and d). Readers are encouraged to note that a non-zero stress relaxation rate is observed in both the experimental data and the model predictions, even when stress magnitudes fall below a representative P91 yield stress value. The estimation of the behaviour would not be possible using an elastic viscoplastic strain decomposition without imposing a physically unrealistic yield stress. An interesting feature of the material response can be observed in these experimental curves. The stress level at the end of the relaxation period is lower for the fast strain rate test ($0.1\%.\ s^{-1}$) than for the slower tests ($0.01\%.\ s^{-1}$ and $0.001\%.\ s^{-1}$), while the total stress drop observed during the strain hold periods increases with increasing strain rate. Fig. 8 e) and f) shows approximately equal relaxation rates at the end of the relaxation periods for all testing strain rates. These observations suggest that all viscous stress curves will converge to the same asymptotic value (the so called equilibrium stress). The definition of this equilibrium stress can be seen in the fourth relaxation period in the second loading cycle in Fig. 8 f). Differences in the asymptotic equilibrium stress value based on loading rate cannot be resolved using the model developed here. The origin of these effects may lie in subtle variations in the material composition between testing samples or the results may be skewed due to grip compliance (“settling”) in the early part of the experiment. A repeatable underlying mechanisms cannot be ruled out however, therefore the above observation is made in order to guide the reader's attention.

Long term cyclic response for intermediate sawtooth type waveforms (i.e. loading waveforms that do not possess strain hold period features) is similarly presented (for loading cycles 100 and 200) in Fig. 9, however σ-t plots are omitted due to limited relevance at this instant. In all cases, an excellent level of agreement is observed between predicted and experimental results, with loading rate dependencies and short/medium/long term viscous effects appropriately represented. Comparisons of stress range are given later in this paper.

5.2. Model validation through sawtooth and dwell responses

Parameter identification for the viscoelastic-viscoplastic model has been achieved in the previous sections using the results generated from anhysteretic loading waveforms only and (as would be expected) a high level of agreement has been observed between model predictions and experimental observations. Elastic/viscoplastic type strain decomposition models have been used extensively in the literature to fit and estimate material response due to more standard waveforms (so-called sawtooth and dwell types, for example) that limit periods of stress relaxation to the end of loading branches (loading direction reversals). This not only demonstrates the applicability of the viscoelastic-viscoplastic formulation but also, for the present sawtooth cases where multiple alternative strain ranges have been used (namely $\pm\ 0.5\%$, $\pm\ 0.4\%$, and $\pm\ 0.25\%$), allows for the validation of hardening behaviour predictions. Note that in all validation results a single loading rate was applied ($0.1\%.\ s^{-1}$). For dwell type validation results, strain hold regions (at 0.5% strain) were limited to $120s$ in duration.

Predicted and experimental material responses for sawtooth type loading waveforms are presented in Fig. 10 (for cycle numbers 2, 50, 100, and 200). Comparative plots for dwell type loading waveforms may be found in Fig. 11 (for cycles 1, 50, 100, and 200). As with the anhysteretic data, σ-t plots are presented that correspond to σ-ε plots, thereby allowing the effects of both material hardening and viscous mechanisms to be easily observed.

5.3. Comments on stress range prediction capability

The prediction of long term stress range evolution during the accumulation of plastic strain is important as it allows for the estimation of the change in yield locus size and provides a useful metric by which to judge the likelihood of yielding in a component (after a known accumulation of plastic strain). From the onset, it was assumed that viscoelastic effects could be decoupled from the isotropic hardening effects, which are thermodynamically associated with the viscoplastic deformation mechanisms. The efficacy of this assumption can be determined by observing the ability of the viscoelastic-viscoplastic model to predict stress range evolution under cyclic loading. Such plots are presented in Fig. 12 for anhysteretic and dwell loading waveforms. The comparison of predicted and experimental responses at various cycle numbers shows a good level of accordance between experimental findings and model predictions; the model can numerically capture the cyclic softening behaviour. However, such behaviour is found slightly under-estimated at low strain rates ($0.01\%.s^{-1}$ and $0.001\%.s^{-1}$), whereas it appears to be correctly predicted at high strain rates ($0.1\%.s^{-1}$)

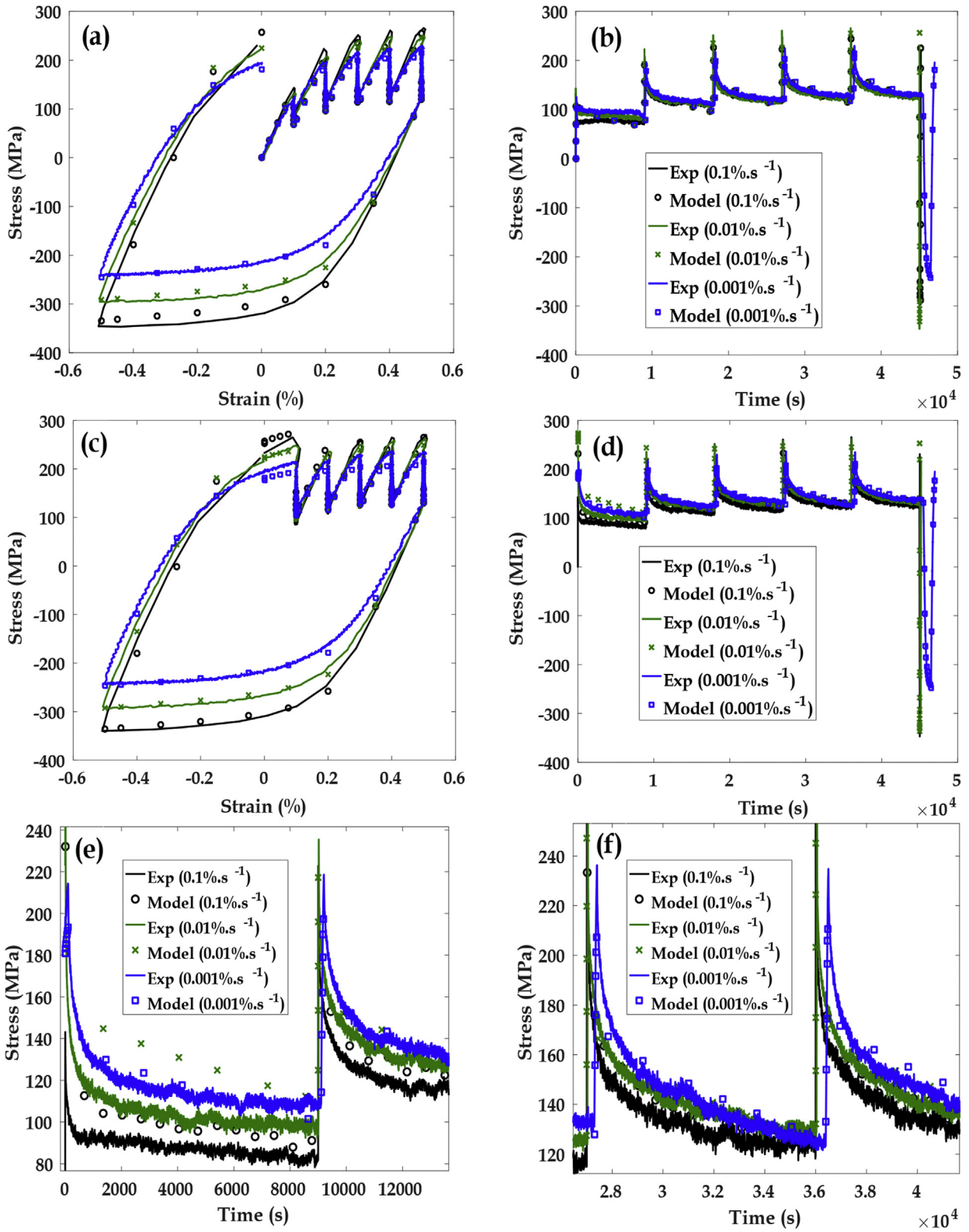

Fig. 8. The prediction of anhysteretic curves using the optimised material parameters (given in Table 3), showing a). $\sigma - \varepsilon$ response in the 1st anhysteretic cycle, b). $\sigma - t$ response in the 1st anhysteretic cycle, c). $\sigma - \varepsilon$ response in the 2nd anhysteretic cycle, d). $\sigma - t$ response in the 2nd anhysteretic cycle, e). the first relaxation period in the 2nd cycle and f) the fourth relaxation period in the 2nd cycle. 2.5 h hold periods were applied during the tensile loading region at strain levels of 0.1%, 0.2%, 0.3%, 0.4%, 0.5%.

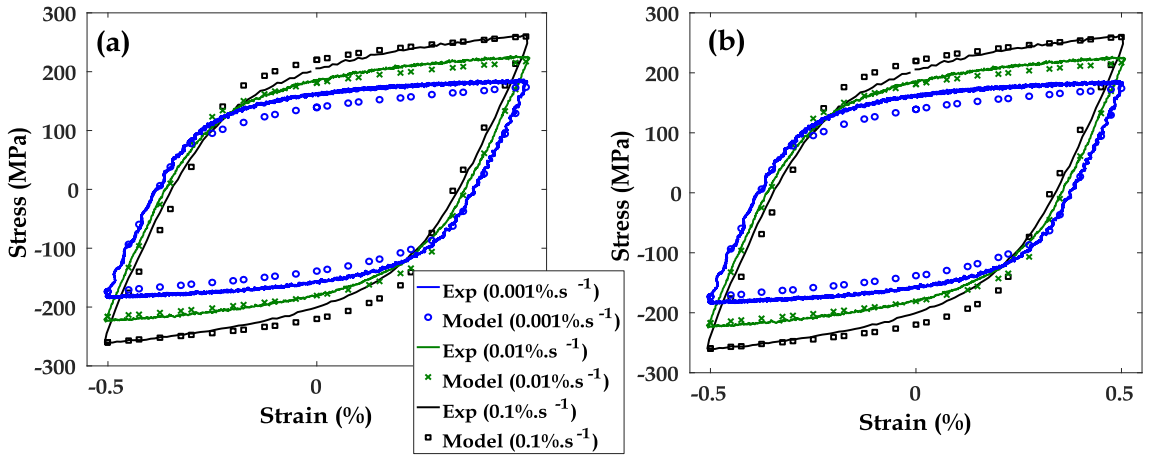

Fig. 9. The prediction of anhysteretic curves and stress range using the optimised material parameters (given in Table 3), showing a). $\sigma - \varepsilon$ response in the 100^{th} anhysteretic cycle and b). $\sigma - \varepsilon$ response in the 200^{th} anhysteretic cycle. The strain amplitude was set at 0.5%.

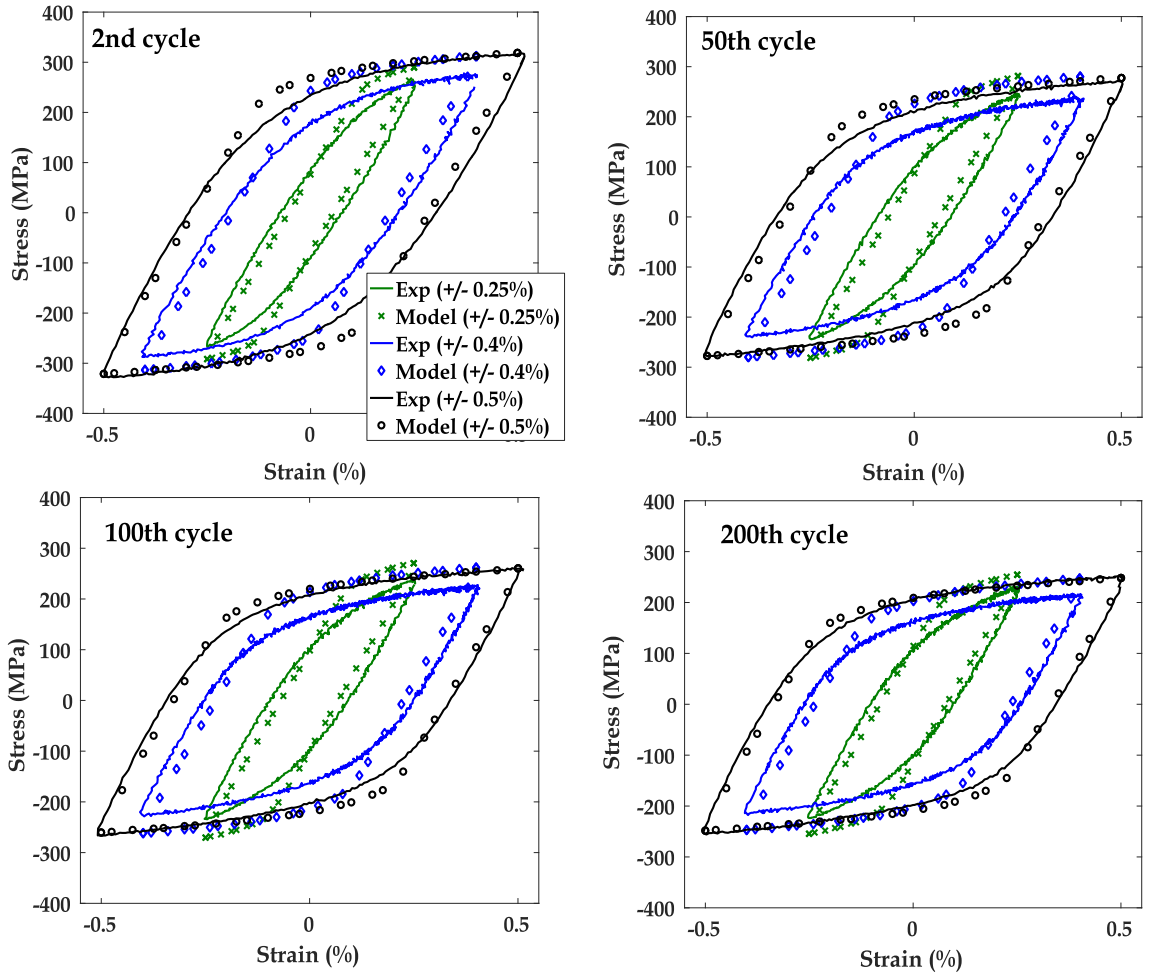

Fig. 10. The prediction of sawtooth curves using the optimised material parameters (given in Table 3), showing $\sigma - \varepsilon$ response in the 2^{nd}, 50^{th}, 100^{th} and 200^{th} of sawtooth cycle. In all cases, results are presented for tests conducted between strain limits of $\pm$ 0.5%, $\pm$ 0.4%, and $\pm$ 0.25% with a strain rate of $0.1\%.s^{-1}$.

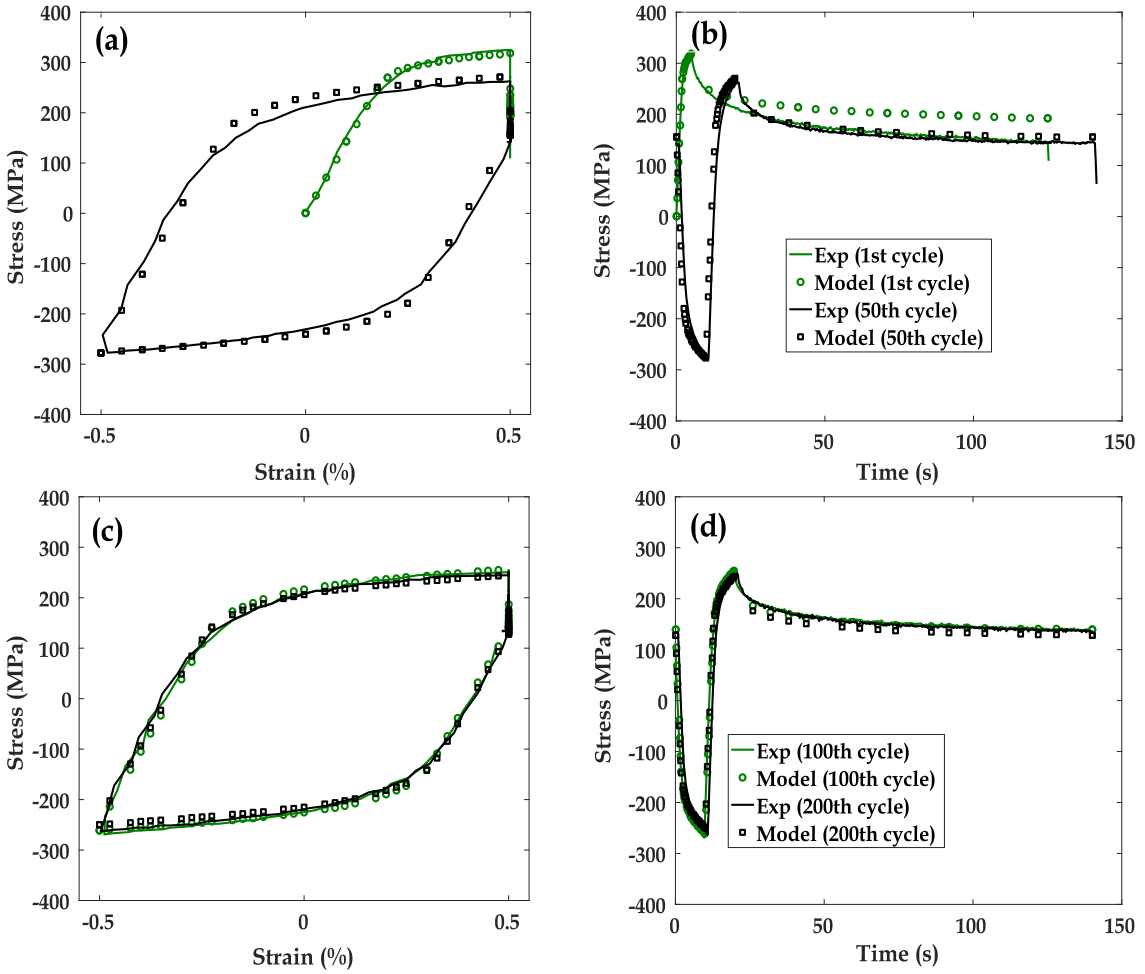

Fig. 11. The prediction of dwell curves using the optimised material parameters (given in Table 3), showing a). $\sigma - \varepsilon$ response in the 1^{st} and 50^{th} dwell cycles, b). $\sigma - t$ response in the 1^{st} and 50^{th} dwell cycles, c). $\sigma - \varepsilon$ response in the 100^{th} and 200^{th} dwell cycles, and d). $\sigma - t$ response in the 100^{th} and 200^{th} dwell cycles. The strain rate was $0.1\%.s^{-1}$ and the strain amplitude was set at 0.5%.

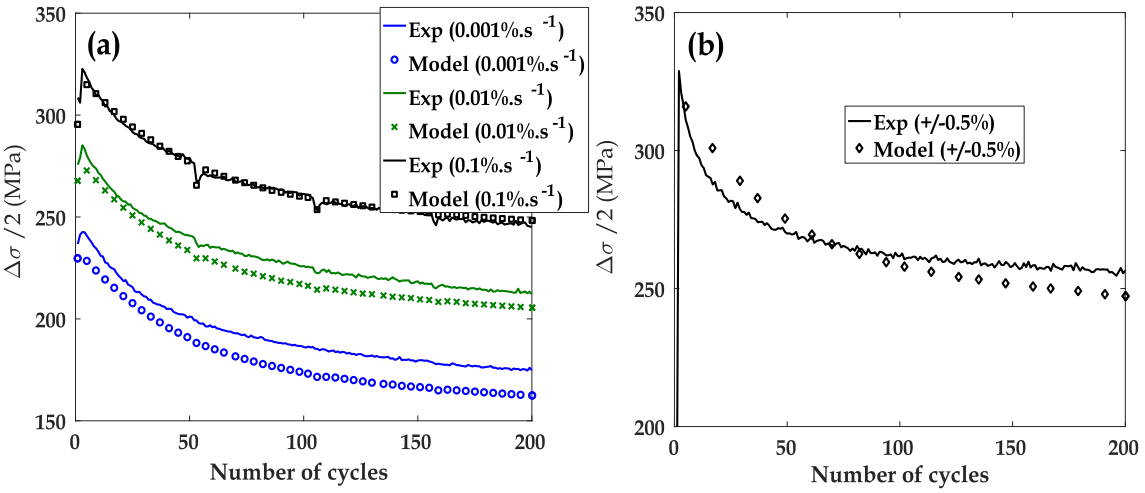

Fig. 12. The prediction of stress amplitude evolution (using the optimised material parameters, see Table 3) for a). anhysteretic (strain limit of $\pm$ 0.5%, loading rates of 0.1%. s^{-1}, 0.01%. s^{-1}, and 0.001%. s^{-1}) and b). dwell (strain limit of $\pm$ 0.5% and a single loading rate of 0.1%. s^{-1} with a 120s hold period at 0.5% strain) waveforms.

for both anhysteretic and dwell cases. The error between the experiment and model prediction becomes important above 50 cycles for low strain rates. This important observation is discussed in the next section.

6. General discussions

The modelling challenge addressed herein is to apply the viscoelastic-viscoplastic model to numerically capture the complex cyclic mechanical behaviour of P91 steels at elevated temperature. The model is mainly developed to describe recoverable viscoelastic effects occurring on short/medium/long times scales, irreversible strains observed above the stress threshold and also nonlinear cyclic softening. However, the main shortcoming of the model is its inability to accurately capture the tensile going loading when small strain ranges are applied; the numerical response seems to be overestimated during both loading and unloading paths for the sawtooth tests. It is not possible, of course, to rule out variations in material composition and texture between testing samples (i.e. between those used for anhysteretic and sawtooth type waveforms), however alternative explanations should be considered. Two back stress components have been applied in the present model formulation, and there is a possibility of a less than optimal partitioning of kinematic hardening components. The ability of the model to predict stresses at peak strains in the anhysteretic, dwell, and sawtooth (at least, in the case of larger loading strain ranges) suggests that saturated values of the back stresses are approximately correct. Over estimation of the stresses at intermediate strains stems from an improper distribution of rate terms associated with each kinematic component. Future work should therefore look to extend the back stress decomposition to include additional, intermediate rate, terms. Alternatively, this drawback can be attributed to the Armstrong-Frederick modelling of the kinematic hardening evolution. The introduction of additional mechanism terms (controlling, say, static recovery) in the adopted kinematic hardening rule would offer another method to refine the predictive capability and accurately capture the hysteresis loop behaviour in the sawtooth tests. Isotropic effects should not be neglected when considering the fact that peak stress values for low strain amplitude sawtooth tests are greatly overestimated. It is possible that some strain range dependency of the cyclic softening (isotropic hardening rules are generally used to capture cyclic softening/hardening phenomenon). Additional features (e.g. time recovery, plastic strain memory) can thus be added to the isotropic hardening rule in order to accurately capture the cyclic reduction in material strength, observed for certain strain amplitudes. For example, the asymptotic value Q_1, related to drag stress, could be made dependent on the plastic strain range in order to account for the memorization of the maximum plastic strain range, as shown experimentally by Zhang and Xuan (2017). The rate sensitivity of cyclic softening may also be better approximated in future iterations of the model. The error between the experimental findings and the simulation becomes significant above 50 cycles for low strain rates. Generally speaking, 9–12% Cr steels exhibit non-linear (followed by linear) cyclic softening, ultimately leading to failure of the material through the continuous accumulation of damage. The model developed herein does not include the effect of fatigue damage and thus cannot reasonably reflect the whole fatigue life of the investigated material. This is not to say the model developed here cannot aid in lifting calculations, as the prediction of more accurate material responses due to periodic excitations can be used to refine estimates made by, say, the well known Coffin-Manson relationship. The introduction of a damage variable (using classical continuum damage mechanics concepts, say) into the isotropic hardening rule would also introduce freedom into the model such that improved response predictions could be made (through non-saturated cyclic softening).

It is also found that the cyclic stress relaxation is slightly overestimated for all strain rates. Although some level of discrepancy can be attributed to aleatory uncertainty (e.g. heat to heat variations), several modelling approaches are at the disposal of researchers for the improvement of the constitutive model to correctly capture the relaxation behaviour and to improve the hardening behaviour prediction at low strain limits. For instance, a static recovery term as introduced by Chaboche (1989) can be added in the kinematic hardening evolution rule to enable stress relaxation at low strain rates. The anhysteretic test waveforms, the long strain hold (relaxation) periods and extended loading application durations (for lower loading rate examples) are considered to be sufficient to highlight the effects of kinematic static recovery. Thus, addition of a static recovery term in the kinematic hardening rule may increase the modelling capability. Since the static recovery may also allow thermal recovery at high temperature, an anisothermal extension of the model is required. Nevertheless, it is well recognized that the correct description of relaxation effects during the dwell period is still one of the most difficult aspects in material behaviour simulation (see Zhang and Xuan (2017), for instance). It is also interesting to mention that all above model predictions are computed under strain-controlled mode with constant strain rates. Thus, it is of great importance to inspect the performance of the viscoelastic-viscoplastic model under stress-controlled mode where the strain rates would vary with loading.

As mentioned above, it is of great important to further extend the model to anisothermal conditions. Indeed, the current model is built under isothermal conditions. Thermodynamics of Irreversible Processes can still be adopted to estimate the heat sources occurring during the fatigue deformation of the investigated material, and thus to complete a fully thermomechanical analysis (see Benaarbia et al. (2014, 2015, 2016)). This needs to experimentally track the evolving of temperature variations during the fatigue process and investigate the dissipative effects and thermomechanical couplings, thereby establishing so-called energy balance (see Benaarbia et al. (2014)). The validation of such a model needs to carefully ascertain aspects of mechanical (hysteresis area and slope, cyclic softening and/or ratcheting strain), thermal (internal heating) and energy responses (dissipation and storage of energy, etc.). This anisothermal analysis can be useful when dealing with cyclic thermal gradients conditions (in thick walled plant components, for instance).

Despite these deficiencies, the current model enables the coupling of viscoelasticity and viscoplasticity and is well grounded in the Thermodynamics of Irreversible Processes and Generalized Standard Materials theory. The model's ability to predict material response has been verified by simulating hysteresis loops for various types of imposed loading waveforms. Referring to the literature on that specific topic, it is rare that models are developed within these foregoing frameworks to investigate the behaviour of high

temperature resistant steels. The viscoelastic-viscoplastic model attempts to describe the isothermal cyclic behaviour with as few parameters as possible. The highly coupled nature of the viscoelastic-viscoplastic mechanisms can make material parameter identification difficult and there is a danger, as in all phenomenological modelling, that the process simply becomes a curve fitting exercise. Although the model presented here is simplified (static recovery is neglected in kinematic terms) a good level of agreement is observed between model predictions and experimental results, regardless of the fact that a range loading rates, ranges, and hold period durations were applied. This suggests that both viscoelastic and viscoplastic mechanisms, which may be effective over long time periods, are represented by the model.

The original motivation for this work was the extension of commonly implemented elastic-viscoplastic constitutive models due to observed phenomenon in P91 component simulations. High temperature deformation phenomenon in chromium steels such as P91 have been explored extensively in the literature at multiple length scales using phenomenological and micro-mechanical approaches (see Kyaw et al. (2016), Rouse et al. (2013), Li et al. (2016b), Li et al. (2014), Siska et al. (2016), Li et al. (2016a)), however attention has been typically limited to short duration (in the order of $1-5$ minutes) viscous effects that are entirely attributed to viscoplastic mechanisms. Significant levels of creep (long term viscous effects) can however be experimentally observed in P91 at $600°C$ for stress much lower than any reasonable interpretation of yield (see Cortellino et al. (2017)), and in many practical implementations of P91 constitutive models (for example, the cyclic analysis of header components in headers, Farragher et al. (2013)) stress magnitudes are in the “elastic” regime. In order to demonstrate the benefit of accounting for viscoelastic strain contributions, Fig. 13 is presented which shows the prediction of the first anhysteretic loading cycle (for all three loading strain rates) assuming an elastic-viscoplastic material model. This simplified model is identical in terms of viscoplasticity to the model developed in the present work, however viscoelastic material parameters in Table 3 (namely η_{v1}, E_{v1}, η_{v2}, E_{v2}, η_{v3}, and E_{v3}) are set to 0. Consequently, no rate dependency can be observed in the initial monotonic loading region of Fig. 13 (elasticity is controlled entirely through the parameter E_0). It can also be observed that, in the model, stress quickly relaxes to an asymptotic value in all strain hold regions. Such effects are entirely expected as viscous effects are limited to the plastic regime of deformation, however they are at odds to the experimental observations.

No optimisation of material parameters has been conducted for the elastic-viscoplastic implementation, therefore comments on predictive capability can only be superficial, however it is worth noting the overestimation of stress in tensile loading regions in Fig. 13. This can be attributed to the improper (non-optimal) partitioning of stress into viscous and back stress contributions (now that viscoelastic effects are neglected). Including or neglecting certain deformation mechanisms can clearly influence other mechanism parameter values due to partitioning and subsequent optimisation. Such effects highlight the need to consider material deformation over a wider range of time scales than those routinely considered for experimental convenience, particularly if results are to be extrapolated in simulations that represent real world conditions.

7. Conclusions

A thermodynamically based viscoelastic-viscoplastic model has been proposed to simulate the mechanical responses of high temperature resistant steels under complex cyclic loading conditions for isothermal environments. The model has been mainly developed for studying fatigue-relaxation interactions at different strain rates/ranges and under varying duration strain hold (stress

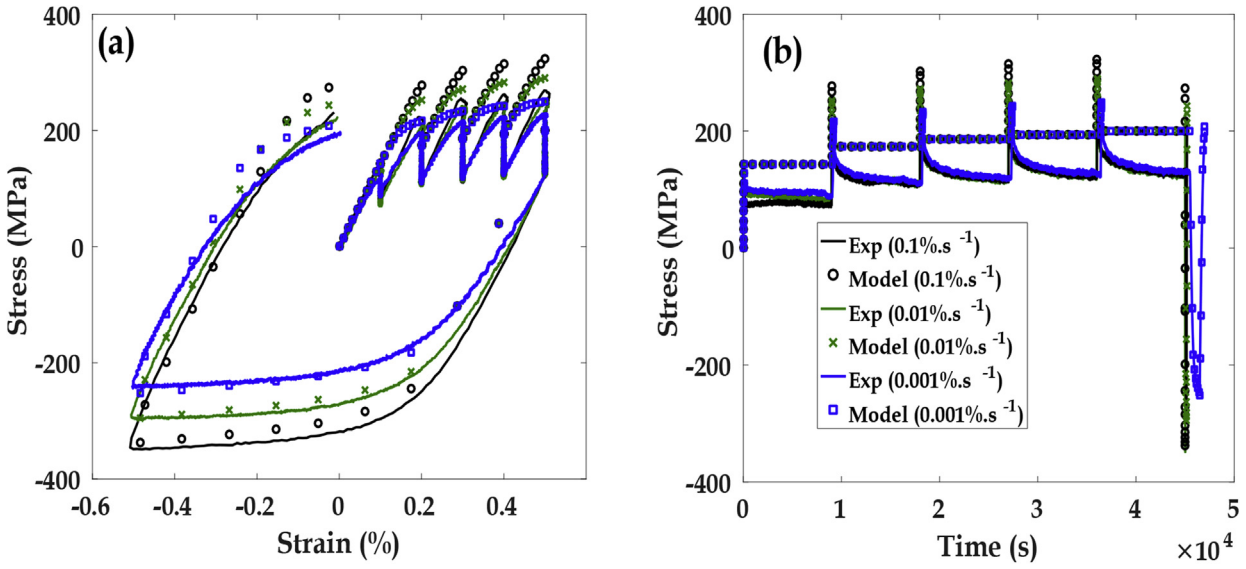

Fig. 13. The predicted material response for anhysteretic loading waveforms, assuming an elastic-viscoplastic material model formulation (for comparison). Responses are shown for the 1^{st} anhysteretic cycle only, highlighting premature viscous stress saturation in a). the $\sigma-\varepsilon$ response and b). the $\sigma-t$ response. As before, the strain amplitude was set at 0.5%.

relaxation) periods. Constitutive equations based on TIP and GSM formalisms are derived from thermodynamic and dissipation potentials. The model combines a hyperbolic sine power viscosity function with non linear isotropic and kinematic hardening rules in order to simulate the experimentally observed irreversible strain evolving above the stress threshold. A great deal of attention was also given to capture the semi-recoverable viscoelastic effects occurring at different time scales (i.e. short, medium and long-term). An uniaxial validation of the constitutive model, based on a heuristic optimisation program combining least-squares function and Levenberg-Marquardt algorithm, is thus developed.

Parameter identification for the viscoelastic-viscoplastic model has been achieved using results generated from anhysteretic loading waveforms. An excellent level of agreement is observed between predicted and experimental results, with loading rate dependencies and short/medium/long term viscous effects appropriately represented. The applicability of the model for the sawtooth and dwell waveform cases, where multiple alternative strain ranges were used, allowed for the validation of hardening behaviour predictions. An in depth examination of the predictive results showed an inability of the model to accurately capture the hardening behaviour when small strain ranges are applied. The predicted responses seem to be overestimated during both loading/unloading paths for the sawtooth case. It is expected that the lack of additional terms in the kinematic and isotropic hardening components has likely led to an overestimation of the kinematic and isotropic conjugate variables, thereby resulting in discrepancies in hardening behaviour for the lowest strain range data. Such effects may also be observed by noting a reduction in the ability of the model to predict hardening behaviour for the lowest strain rate data. Despite this, a significant adverse effect in viscous behaviour prediction in not observed (evidenced by the ability of the predict asymptotic and transient stress relaxation behaviour in Figs. 9 and 11). The effects of long term stress relaxation/inelastic strain accumulation is not commonly investigated in work of this type, particularly for P91. This behaviour is however important in many industrial application, particularity in a modern world were societal pressures are driving for sustainability and economic responsibility.

Based on the comments made above, future developments will focus on the inclusion of hardening terms (thereby requiring a robust initial estimation procedure to be implemented) to improve the cyclic hardening and the decelerated stress relaxation behaviour for a variety of strain ranges. Anisothermal and thermo-mechanical coupling effects should also be quantified in future model iterations through the analysis of appropriate (new) experimental data and the development of Taylor-Quinney coefficient relationships. Work should also be undertaken focusing on the incorporation of microstructural features in the model constitutive equations. The inclusion of such information in the constitutive relationships will enhance the fundamental understanding that the model can provide (for complex highly coupled behaviour mechanisms) and assist in guarding against models becoming “curve fitting” methods. Dislocation mechanics based constitutive equations can be used to deeply consider effects such strain hardening, strain-rate dependencies and thermal softening.

Acknowledgements

The authors gratefully acknowledge *the Engineering and Physical Research Council (EPSRC)* for supporting this work. This work was performed under the framework of the Flex-E-Plant project (Grant number: EP/K021095/1) and IMPULSE project (grant number EP/N509991/1).).

We also thank the following partners for their the valuable contributions: GE Power, Doosan Babcock Limited, Centrica plc., EDF Energy (West Burton Power) Limited, Uniper Technologies Limited, Goodwin Steel Castings Limited, NPL Management Limited, R-MC Power Recovery Limited, RWE Generation UK plc., Scottish and Southern Energy (SSE) plc., Siemens Industrial Turbomachinery and TWI Limited.

Appendix A. Supplementary data

Supplementary data related to this article can be found at http://dx.doi.org/10.1016/j.ijplas.2018.03.015.

References

Abdel-Karim, M., 2009. Modified kinematic hardening rules for simulations of ratchetting. Int. J. Plast. 25 (8), 1560–1587.
Ahmed, R., Barrett, P.R., Hassan, T., 2016. Unified viscoplasticity modeling for isothermal low-cycle fatigue and fatigue-creep stress-strain responses of haynes 230. Int. J. Solid Struct. 88–89, 131–145.
Al-Rub, R.K.A., Darabi, M.K., 2012. A thermodynamic framework for constitutive modeling of time- and rate-dependent materials. part i: Theory. Int. J. Plast. 34, 61–92.
Armstrong, P.J., Frederick, C.O., 1966. A Mathematical Representation of the Multiaxial Bauschinger Effect. Central Electricity Generating Board, Berkeley Nuclear Laboratories, Research and Development Department CEGB Report No. RD/B/N 731.
Barrett, R., O'Donoghue, P., Leen, S., 2013. An improved unified viscoplastic constitutive model for strain-rate sensitivity in high temperature fatigue. Int. J. Fatig. 48, 192–204.
Benaarbia, A., Chrysochoos, A., Robert, G., 2014. Kinetics of stored and dissipated energies associated with cyclic loadings of dry polyamide 6.6 specimens. Polym. Test. 34, 155–167.
Benaarbia, A., Chrysochoos, A., Robert, G., 2015. Influence of relative humidity and loading frequency on the pa6.6 thermomechanical cyclic behavior: Part ii. energy aspects. Polym. Test. 41, 92–98.
Benaarbia, A., Chrysochoos, A., Robert, G., 2016. Thermomechanical analysis of the onset of strain concentration zones in wet polyamide 6.6 subjected to cyclic loading. Mech. Mater. 99, 9–25.
Cailletaud, G., Sai, K., 1995. Study of plastic/viscoplastic models with various inelastic mechanisms. Int. J. Plast. 11 (8), 991–1005.
Chaboche, J., 1989. Constitutive equations for cyclic plasticity and cyclic viscoplasticity. Int. J. Plast. 5 (3), 247–302.
Chaboche, J., 2008. A review of some plasticity and viscoplasticity constitutive theories. Int. J. Plast. 24 (10), 1642–1693 special Issue in Honor of Jean-Louis Chaboche.
Chaboche, J., Rousselier, G., 1983. On the plastic and viscoplastic constitutive equations - part i: rules developed with internal variable concept. ASME J. Pressure

Vessel Technol. 105, 153–158.
Chaboche, J.-L., 1997. Thermodynamic formulation of constitutive equations and application to the viscoplasticity and viscoelasticity of metals and polymers. Int. J. Solid Struct. 34 (18), 2239–2254.
Chatzigeorgiou, G., Charalambakis, N., Chemisky, Y., Meraghni, F., 2016. Periodic homogenization for fully coupled thermomechanical modeling of dissipative generalized standard materials. Int. J. Plast. 81, 18–39.
Chen, R., Armaki, H.G., Maruyama, K., Igarashi, M., 2011. Long-term microstructural degradation and creep strength in gr.91 steel. Mater. Sci. Eng. A 528 (13), 4390–4394.
Chen, X., Jiao, R., 2004. Modified kinematic hardening rule for multiaxial ratcheting prediction. Int. J. Plast. 20 (4), 871–898.
Contesti, E., Cailletaud, G., 1987. Description of creep-plasticity interaction with non-unified constitutive equations: application to an austenitic stainless steel. In: 6th International Seminar on Inelastic Analysis and Life Prediction in High Temperature Environment.
Cortellino, F., Rouse, J.P., Cacciapuoti, B., Sun, W., Hyde, T.H., 2017. Experimental and numerical analysis of initial plasticity in p91 steel small punch creep samples. Exp. Mech. 57, 1193–1212.
Cottrell, A., 1953. Dislocations and Plastic Flow in Crystals. Oxford University, London.
Cui, L., Wang, P., Hoche, H., Scholz, A., Berger, C., 2013. The influence of temperature transients on the lifetime of modern high - chromium rotor steel under service-type loading. Mater. Sci. Eng. A 560, 767–780.
Darabi, M.K., Rub, R.K.A.A., Masad, E.A., Huang, C.-W., Little, D.N., 2011. A thermo-viscoelastic - viscoplastic - viscodamage constitutive model for asphaltic materials. Int. J. Solid Struct. 48 (1), 191–207.
Farragher, T., Scully, S., O'Dowd, N., Leen, S., 2013. Development of life assessment procedures for power plant headers operated under flexible loading scenarios. Int. J. Fatig. 49, 50–61.
Fournier, B., Sauzay, M., Caës, C., Noblecourt, M., Mottot, M., 2006. Analysis of the hysteresis loops of a martensitic steel: Part i: study of the influence of strain amplitude and temperature under pure fatigue loadings using an enhanced stress partitioning method. Mater. Sci. Eng. A 437 (2), 183–196.
Fournier, B., Sauzay, M., Caes, C., Noblecourt, M., Mottot, M., Bougault, A., Rabeau, V., Pineau, A., 2008a. Creep - fatigue - oxidation interactions in a 9cr - 1mo martensitic steel. part i: effect of tensile holding period on fatigue lifetime. Int. J. Fatig. 30 (4), 649–662.
Fournier, B., Sauzay, M., Caes, C., Noblecourt, M., Mottot, M., Bougault, A., Rabeau, V., Pineau, A., 2008b. Creep - fatigue - oxidation interactions in a 9cr - 1mo martensitic steel. part ii: effect of compressive holding period on fatigue lifetime. Int. J. Fatig. 30 (4), 663–676.
Fournier, B., Sauzay, M., Pineau, A., 2011. Micromechanical model of the high temperature cyclic behavior of 9-12%cr martensitic steels. Int. J. Plast. 27 (11), 1803–1816.
Gudimetla, M.R., Doghri, I., 2017. A finite strain thermodynamically-based constitutive framework coupling viscoelasticity and viscoplasticity with application to glassy polymers. Int. J. Plast. 98 (Suppl. C), 197–216.
Haddag, B., Meraim, F.A., Balan, T., 2009. Strain localization analysis using a large deformation anisotropic elastic - plastic model coupled with damage. Int. J. Plast. 25 (10), 1970–1996.
Halphen, B., Nguyen, Q., 1975. On the generalized standards materials (in French). J. Mec. 14, 39–63.
Kang, G., Kan, Q., 2007. Constitutive modeling for uniaxial time-dependent ratcheting of ss304 stainless steel. Mech. Mater. 39 (5), 488–499.
Kang, G., Ohno, N., Nebu, A., 2003. Constitutive modeling of strain range dependent cyclic hardening. Int. J. Plast. 19 (10), 1801–1819.
Kyaw, S.T., Rouse, J.P., Lu, J., Sun, W., 2016. Determination of material parameters for a unified viscoplasticity-damage model for a p91 power plant steel. Int. J. Mech. Sci. 115, 168–179.
Launay, A., Maitournam, M., Marco, Y., Raoult, I., Szmytka, F., 2011. Cyclic behaviour of short glass fibre reinforced polyamide: experimental study and constitutive equations. Int. J. Plast. 27 (8), 1267–1293.
Lemaitre, J., 1985. Coupled elasto-plasticity and damage constitutive equations. Comput. Meth. Appl. Mech. Eng. 51 (1), 31–49.
Lemaitre, J., Chaboche, J., 2000. Mechanics of Solid Materials. Cambridge University Press, Cambridge.
Li, D.-F., Barrett, R.A., O'Donoghue, P.E., Hyde, C.J., O'Dowd, N.P., Leen, S.B., 2016a. Micromechanical finite element modelling of thermo-mechanical fatigue for p91 steels. Int. J. Fatig. 87, 192–202.
Li, D.-F., Golden, B.J., O'Dowd, N.P., 2014. Multiscale modelling of mechanical response in a martensitic steel: a micromechanical and length-scale-dependent framework for precipitate hardening. Acta Mater. 80, 445–456.
Li, M., Barrett, R.A., Scully, S., Harrison, N.M., Leen, S.B., O'Donoghue, P.E., 2016b. Cyclic plasticity of welded p91 material for simple and complex power plant connections. Int. J. Fatig. 87, 391–404.
Nguyen, Q., 1973. Matériaux élastoviscoplastiques a potentiel généralisé. C. R. Acad. Sci. 277 (8), 915–918.
Ohno, N., Wang, J.-D., 1993. Kinematic hardening rules with critical state of dynamic recovery, part i: formulation and basic features for ratchetting behavior. Int. J. Plast. 9 (3), 375–390.
Pineau, A., Antolovitch, S., 2015. High temperature fatigue: behaviour of three typical classes of structural materials. Mater. A. T. High. Temp. 32, 298–317.
Prager, W., 1949. Recent developments in the mathematical theory of plasticity. J. Appl. Phys. 20 (235).
Ranc, N., Chrysochoos, A., 2013. Calorimetric consequences of thermal softening in johnson - cook's model. Mech. Mater. 65, 44–55.
Rouse, J.P., Hyde, C.J., Sun, W., Hyde, T.H., 2013. Comparison of several optimisation strategies for the determination of material constants in the chaboche visco-plasticity model. J. Strain Anal. Eng. Des. 48, 347–363.
Saad, A., Hyde, T., Sun, W., Hyde, C., Tanner, D., 2013. Characterization of viscoplasticity behaviour of p91 and p92 power plant steels. Int. J. Pres. Ves. Pip. 111, 246–252.
Shankar, V., Mariappan, K., Sandhya, R., Laha, K., Bhaduri, A., 2017. Long term creep-fatigue interaction studies on India-specific reduced activation ferritic-martensitic (in-rafm) steel. Int. J. Fatig. 98, 259–268.
Siska, F., Stratil, L., Smid, M., Luptakova, N., Zalezak, T., Bartkova, D., 2016. Deformation and fracture behavior of the p91 martensitic steel at high temperatures. Mater. Sci. Eng., A 672, 1–6.
Swindeman, R., Santella, M., Maziasz, P., Roberts, B., Coleman, K., 2004. Issues in replacing cr-mo steels and stainless steels with 9cr-1mo-v steel. Int. J. Pres. Ves. Pip. 81 (6), 507–512 the 7th International Conference on Operating Pressure Equipment.
Tong, J., Vermeulen, B., 2003. The description of cyclic plasticity and viscoplasticity of waspaloy using unified constitutive equations. Int. J. Fatig. 25, 413–420.
Velay, V., Bernhart, G., Penazzi, L., 2006. Cyclic behavior modeling of a tempered martensitic hot work tool steel. Int. J. Plast. 22 (3), 459–496.
Viswanathan, R., Henry, J., Shingledecker, J., Vitalis, B., Purgert, R., 2005. U.s. program on materials technology for ultra-supercritical coal power plants. J. Mater. Eng. Perform. 14, 281–292.
Voyiadjis, G.Z., Dorgan, R.J., 2007. Framework using functional forms of hardening internal state variables in modeling elasto-plastic-damage behavior. Int. J. Plast. 23 (10), 1826–1859 in honor of Professor Dusan Krajcinovic.
Wang, J., Steinmann, P., Rudolph, J., Willuweit, A., 2015. Simulation of creep and cyclic viscoplastic strains in high - cr steel components based on a modified becker - hackenberg model. Int. J. Pres. Ves. Pip. 128, 36–47.
Wang, W., Buhl, P., Klenk, A., 2014. A unified viscoplastic constitutive model with damage for multi-axial creep-fatigue loading. Int. J. Damage Mech. 24, 363–382.
Xu, L., Zhao, L., Gao, Z., Han, Y., 2017. A novel creep - fatigue interaction damage model with the stress effect to simulate the creep - fatigue crack growth behavior. Int. J. Mech. Sci. 130, 143–153.
Yaguchi, M., Yamamoto, M., Ogata, T., 2002. A viscoplastic constitutive model for nickel-base superalloy, part 1: kinematic hardening rule of anisotropic dynamic recovery. Int. J. Plast. 18 (8), 1083–1109.
Yu, C., Kang, G., Chen, K., 2017. A hygro-thermo-mechanical coupled cyclic constitutive model for polymers with considering glass transition. Int. J. Plast. 89, 29–65.
Yu, C., Kang, G., Lu, F., Zhu, Y., Chen, K., 2016. Viscoelastic-viscoplastic cyclic deformation of polycarbonate polymer: experiment and constitutive model. J. Appl. Mech. 83, 041002.
Zhang, K., Aktaa, J., 2016. Characterization and modeling of the ratcheting behavior of the ferritic - martensitic steel p91. J. Nucl. Mater. 472, 227–239.
Zhang, S.-L., Xuan, F.-Z., 2017. Interaction of cyclic softening and stress relaxation of 9-12% cr steel under strain-controlled fatigue-creep condition: experimental and modeling. Int. J. Plast. 98, 45–64.
Zhu, Y., Kang, G., Yu, C., 2017. A finite cyclic elasto-plastic constitutive model to improve the description of cyclic stress-strain hysteresis loops. Int. J. Plast. 95, 191–215.